

5101-282  
Flat-Plate  
Solar Array Project

DOE/JPL-1012-118  
Distribution Category UC-63b

# The Influence of Environmental Parameters on the Thermal Performance of Photovoltaic Arrays

L.C. Wen

October 15, 1985

Prepared for

**U.S. Department of Energy**  
Through an Agreement with  
**National Aeronautics and Space Administration**

by

**Jet Propulsion Laboratory**  
California Institute of Technology  
Pasadena, California

JPL Publication 85-94

Prepared by the Jet Propulsion Laboratory, California Institute of Technology,  
for the U.S. Department of Energy through an agreement with the National  
Aeronautics and Space Administration.

The JPL Flat-Plate Solar Array Project is sponsored by the U.S. Department of  
Energy and is part of the National Photovoltaics Program to initiate a major  
effort toward the development of cost-competitive solar arrays.

This report was prepared as an account of work sponsored by an agency of the  
United States Government. Neither the United States Government nor any  
agency thereof, nor any of their employees, makes any warranty, express or  
implied, or assumes any legal liability or responsibility for the accuracy, com-  
pleteness, or usefulness of any information, apparatus, product, or process  
disclosed, or represents that its use would not infringe privately owned rights.

Reference herein to any specific commercial product, process, or service by trade  
name, trademark, manufacturer, or otherwise, does not necessarily constitute or  
imply its endorsement, recommendation, or favoring by the United States  
Government or any agency thereof. The views and opinions of authors expressed  
herein do not necessarily state or reflect those of the United States Government  
or any agency thereof.

This document reports on work done under NASA Task RE-152, Amendment  
419, DOE/NASA IAA No. DE-A101-85CE89008.

## ABSTRACT

Results of a detailed investigation of thermal testing and computer simulation of a representative photovoltaic module are presented. The objective of the study is to assess the influence of environmental parameters. Existing analytical correlations describing the effects of primary environmental factors, including solar irradiance, ambient temperature and wind conditions are verified with experimental results and are found to be adequate. The common source of error found in NOCT test evaluation and PV module performance simulation appears to be related to secondary environmental factors such as the changes in ground reflection, ground infrared emission and sky radiation. In past practices the effects of these factors were not properly included. Consequently, an uncertainty band of 3 to 5 degrees Celsius are often observed in typical NOCT data evaluation.

In the present investigation a series of special experiments are designed and conducted. Detailed calibrations and verifications are made to delineate the effects of all the environmental factors such that the observed uncertainty band can be minimized. Upgraded thermal models using refined heat transfer correlations are developed in the report. The resultant computer model are verified by comparing transient thermal simulation of the selected module with experimental measurements. The standard deviation between analysis and experimental data for the sample cases is demonstrated to be around 1 degree C.

#### ACKNOWLEDGEMENTS

The author wishes to thank, R. Weaver, D. Berns, J. Gomez and J. Griffith for their assistance in this investigation, M. Fuentes and D. McClesse for suggestions in sky radiation evaluation.

This publication reports on work done under NASA Task RD-152, Amendment 66,DOE/NASA IAA No. DE-AI01-76ET20356.

## GLOSSARY

### ABBREVIATION AND ACRONYMS

ASEC	Applied Solar Electric Corp.
DOE	U.S.Department of Energy
FSA	Flat Plate Solar Array (Project)
JPL	Jet Propulsion Laboratory
NASA	National Aeronautics and Space administration
NOCT	Nominal Operating Cell Temperature
NTE	Nominal Thermal Environment
PV	Photovoltaic(s)

### DEFINITION OF SYMBOLS

Symbols	Description	Units
A	area	$m^2$
B	sky IR radiation function	$W/m^2$
C	unit conductance	$W/m^2-C$
$C_p$	specific heat	Wh/kg
$D^p$	wind distribution function	
E	infrared emission	$W/m^2$
f	anisotropic sky radiation	
H	forced convection coefficient	$W/m^2-C$
h	free convection coefficient	$W/m^2-C$
$L_d$	isotropic horizontal sky radiation	$W/m^2$
M	mass	kg
Q	thermal power	W
S	solar irradiance	$W/m^2$
T	temperature	C
t	time	h,min,sec
V	effective wind speed	m/s
$\alpha$	solar absorptance	
$\epsilon$	surface emittance	
$\theta$	module tilt angle	degrees
$\sigma$	Stefan-Boltzmann constant	$W/m^2-K^4$
$\omega$	wind direction	degrees
$\gamma$	water vapor pressure in moist air	

#### Subscripts

a	ambient
b	back surface
c	conduction
dp	dew point
f	front surface
g	ground
r	radiation
s	sky

## CONTENTS

### I. INTRODUCTION

### II. REVIEW OF FUNDAMENTALS

#### A. ANALYTICAL METHODOLOGY AND HEAT TRANSFER CORRELATIONS

- (1) Module Thermophysical Properties
- (2) Convective Heat Transfer
- (3) Radiative Heat Transfer

#### B. CORRELATING ANALYTICAL AND EXPERIMENTAL RESULTS

- (1) Experimental Observation
- (2) Transient Simulation
- (3) Assessment of Uncertainties

### III. EXPERIMENTAL INVESTIGATION

#### A. EXPERIMENTAL SET-UP

- (1) Test Site and Environmental Conditions
- (2) Test Hardware and Sensor Calibrations

#### B. GROUND EMISSION

#### C. SKY RADIATION

### IV. MODEL VERIFICATION AND DISCUSSION

#### A. TRANSIENT SIMULATION

#### B. ENERGY BALANCE RELATIONSHIP

#### C. DISCUSSION

### V. REFERENCES

## FIGURES

- Fig. II-1      Representative Thermal Network Models
- Fig. II-2      Spectral Reflectance Measurements of Cell surfaces
- Fig. II-3.     Distribution Function of Forced Air Convection
- Fig. II-4.     Representative Cell Temperature Profiles
- Fig.III-1.    Overview of JPL Thermal Test Site
- Fig.III-2.    Representative Wind Speed Variations at the Test Site
- Fig.III-3.    Typical Wind Direction Variations at the Test Site, (a) West Anemometer and (b) East Anemometer.
- Fig.III-4.    Correlations between Pyranometer Readings and Solar Cell Measurements
- Fig.III-5.    Comparisons of Direct (Front) Solar Irradiance and Ground Reflection
- Fig.III-6.    Ambient Temperature Profiles
- Fig.III-7.    Ground Temperature Distributions
- Fig.III-8.    Atmospheric Radiation from a Cloudless Sky
- Fig.III-9.    Atmospheric Radiation from a Cloudy Sky
- Fig. IV-1.    Transient Simulation on January 15, 1984
- Fig. IV-2.    Transient Simulation on November 28, 1983
- Fig. IV-3.    Solar Energy Absorption by Module Surfaces
- Fig. IV-4.    Infrared Energy Exchanges
- Fig. IV-5.    Heat Losses from the Module Surfaces
- Fig. IV-6.    Instantaneous Thermal Energy Balance
- Fig. IV-7.    Simulated Cell Temperature Profiles under NTE Conditions

## SECTION I

### INTRODUCTION

The electrical power output, and more importantly the lifetime, of photovoltaic arrays are functions of cell temperature. Because of this temperature dependency it is important to have a thorough understanding of the thermal performance of photovoltaic modules. The concept of NOCT (Nominal Operating Cell Temperature) was introduced in 1976 (Ref. 1) and has since been widely accepted as a simple measure of module thermal characteristics. Analytical thermal modelling is another commonly applied technique employed to predict module thermal performance. Transient module temperature simulation, with parameters adjusted to match corresponding experimental measurements, has been found to be very useful in determining the effects of underlying design parameters for different residential array mounting concepts (Ref. 2).

Although the process of NOCT testing/evaluation and the thermal model simulation of module performance have both become common practices, they are not, however, without minor problems. Typical NOCT test data are scattered within a band of 5 to 7 degrees C. Long term test data base are sometimes required to filter the random variation in order to achieve a statistically meaningful value. For instance, the NOCT evaluation process for the Block IV PV modules made use of test data collected in a time span over six months.

One anomaly that has often been observed in past NOCT test data evaluation is the AM-PM differences. NOCT values based on data recorded in the afternoon were reported to be different from those based on the morning data (Ref. 3). Although the discrepancy was usually less than 2 to 3 degrees Celsius, it nevertheless demonstrates that some of the environmental changes were not properly accounted for. Similar discrepancy occurred in transient thermal simulations. In many cases the resultant thermal model produces very close approximation of the test data and yet the same model would generate persistent temperature deviations between the simulated and the measured results when a different set of experimental data was used.

A review of past experimental results indicates that some of the discrepancies were caused by experimental errors and others were due to the fact that many secondary environmental factors were not included in the test evaluation process. The current established thermal characterization process only takes into considerations the major environmental parameters: solar irradiance, ambient temperature and wind conditions. While these are the dominating environmental factors that govern PV module thermal performance, they do not represent a complete set of boundary condition specifications that enable one to simulate the module thermal behavior satisfactorily.

The Jet Propulsion Laboratory's (JPL) Flat-plate Solar Array project (FSA) has been engaged in development of test methods and design approaches for flat plate arrays and modules. One of the objectives for current thermal activities is to refine the NOCT test/evaluation procedure and to provide simple and accurate algorithms for predicting array thermal performance. In order to eliminate serious discrepancies in test data evaluation and to improve

the accuracy in analytical predictions, the major thrust of the current thermal activity is to establish a thorough assessment of the effects of environmental parameters, especially those due to the often ignored secondary factors.

## SECTION II

### REVIEW OF FUNDAMENTALS

The present thermal investigation of PV modules is aimed to minimize the uncertainties commonly involved in test evaluation process and in analytical predictions. The study approach consists of three sequential phases. Current practices of experimental procedures and analytical heat transfer correlations are examined first to identify possible sources of error that could result in the observed discrepancies. A special series of experiments can then be conducted, in the second phase, to resolve these issues. Based on the experimental findings, one can improve the test procedures in reducing experimental errors and the same data set is used to calibrate pertinent heat transfer correlations used in performing thermal analysis. Thermal models can be refined to generate more reliable predictions. Final verification of the heat transfer correlations used in the resultant model is performed by comparing the simulated temperature predictions with actual module temperature measurements.

#### A. ANALYTICAL METHODOLOGY AND HEAT TRANSFER CORRELATIONS:

The influence of environmental parameters to the thermal performance of a PV module is governed by the energy balance equation shown in Equation (II-1). Under no load (open circuit) test conditions, the amount of absorbed solar energy is set to be equal to the sum of heat losses to the ambient and the change in thermal energy content.

$$A (\alpha_f + \alpha_b) S = Q_c + Q_r + MC_p \frac{dT}{dt} \quad (\text{II-1})$$

where

A = effective module area

$\alpha_f$  ,  $\alpha_b$  = effective solar absorptance for the front and rear surfaces

S = solar irradiance

$Q_c$  = Convective heat loss to the ambient

$Q_r$  = Radiative heat loss

$MC_p$  = thermal capacitance of module

T = module temperature

t = time

Equation (II-1) shows the energy balance of a single-node thermal system. Detailed thermal modelling analysis using thermal analyzer programs such as SINDA (Ref. 4) usually employs multi-node models to account for individual component responses. Figure II-1 illustrates two network models, representing different levels of detail, for a rack-mounted PV module.

In the following, the major components involved in module energy balance are discussed. They can be categorized into three groups: (1) module thermophysical properties such as solar absorptance, surface emittance, conductance, etc (2) convective heat loss and (3) radiative heat loss. Heat transfer between the module and the ambient is governed by many environmental parameters. Some are conventional meteorological quantities such as solar irradiance, ambient temperature and wind conditions. Others are implicit factors that are peculiar to the test site or to the test configuration. These include the ground characteristics, the module tilt angle and the wind interference by local structures.

#### (1) Module Thermophysical Properties:

##### (a) Solar Absorptance and Emittance:

Since the active surface of a module consists of composite layers of cell ensembles, encapsulant and interconnectors, the thermal optical properties of the module are represented by effective composite values of solar absorptances and emittances. The individual solar absorptance component can be computed from spectral reflectance measured in the wavelength range between 0.28 to 2.5 microns. The solar absorptance of cells can be significantly modified by surface coating applications. Figure II-2 (Ref. 5) shows the spectral reflectance measurements for the front cell surfaces of two commercially manufactured modules. For the Motorola module (model MSP43E40B) the measured solar absorptances, integrated using an AM2 (air mass two) solar spectrum, are reported to be 0.92 for the cell surface, 0.73 for the intercell spaces and 0.39 for the rear module surface. In contrast, the corresponding solar absorptance of the ASEC cell is only 0.8 as a result of the high reflectance in the 1 to 2 micron region, which is caused by a BSR (Back Surface Reflector) coating application.

Infrared emittance of the module surfaces is determined by long wave length (greater than 2.5 microns) radiative characteristics. The effective emittances of the ASEC and the Motorola modules are about the same, with values around 0.83 for both the front and rear surfaces.

##### (b) Thermal Inertia

If the module has a negligible thermal mass, its temperature would track the instantaneous changes in environmental conditions. This is usually referred to as an 'arithmetic' nodal temperature. However, in reality, the temperature response for most PV module designs are far from being 'arithmetic'. The time constant for most PV modules is around 4 to 20 minutes, depending on the thermal design and mounting configurations. For example, the specific thermal capacitance for the Motorola module is evaluated to be 3.6 W-h/C per square meter module area, based on the specifications shown in reference 6. The corresponding time constant is around 6 minutes.

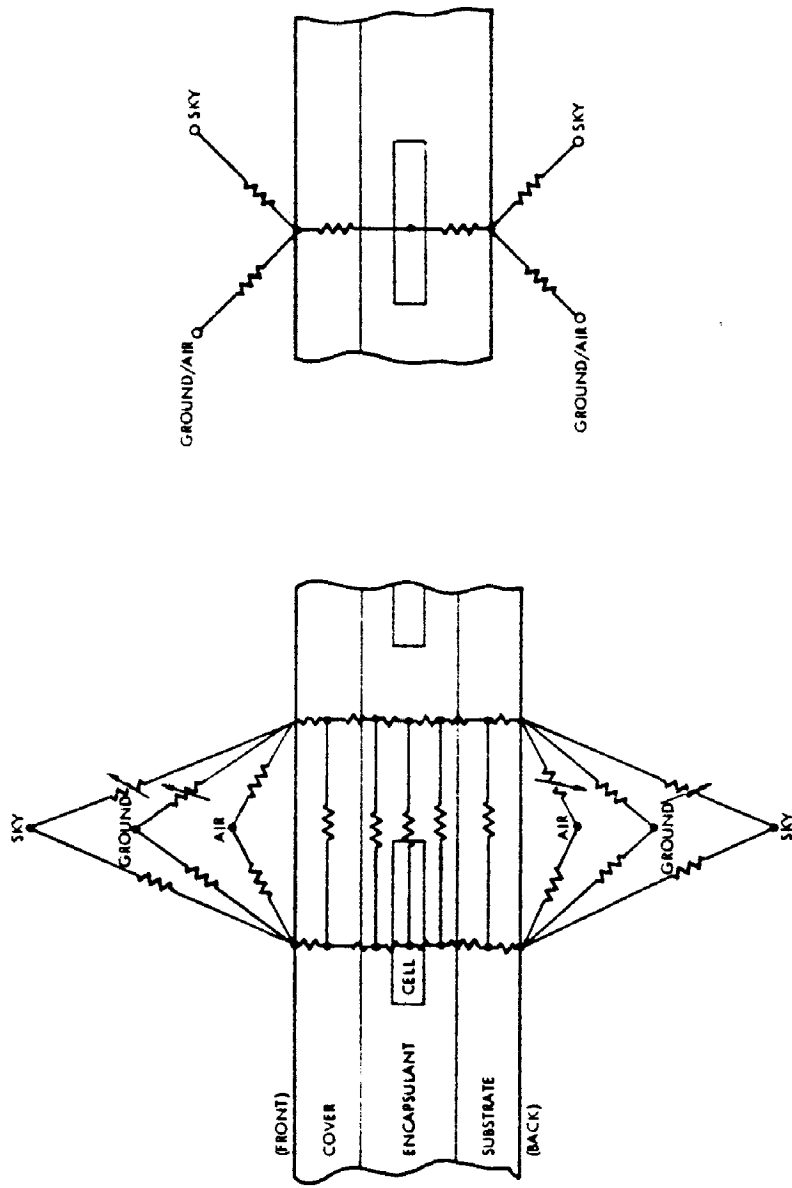


Fig. II-1 Representative Thermal Network Models

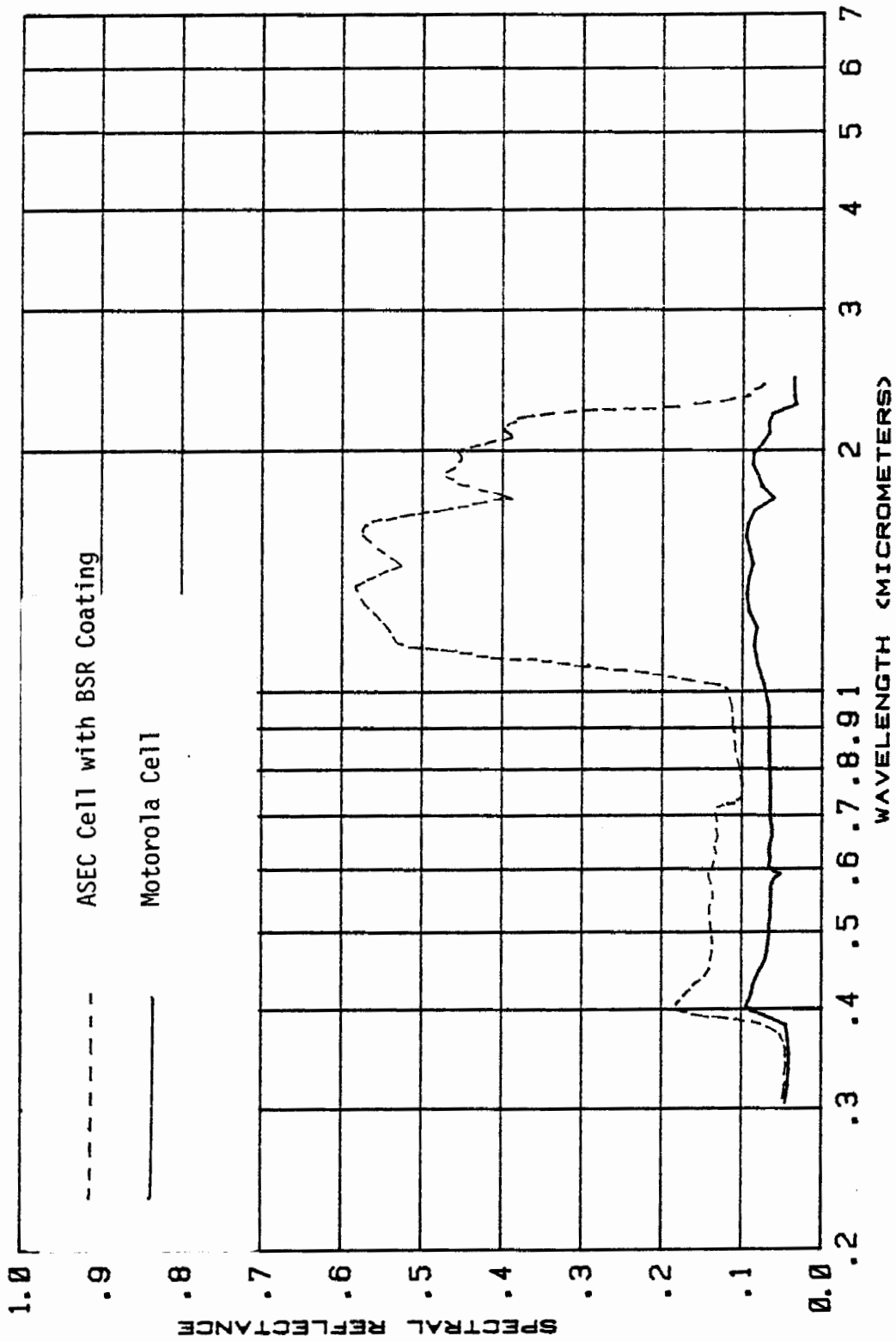


Fig. II-2 Spectral Reflectance Measurements of Cell Surfaces

(2) Convective Heat Transfer:

Convective heat transfer between the module and its natural environment is affected by many parameters. Turbulent wind conditions and the interaction between free and forced convection cause large uncertainties in convective heat transfer predictions. Many heat transfer correlations have been suggested for free convections (Refs. 7,8) and forced convection (Refs. 9,10,11,12). For wind speed greater than 5 m/s forced convection dominates. For wind speed less than 5 m/s, superposition of the individual effects of free and forced convection, as shown in equation (II-2), appears to yield satisfactory results.

$$Q_c = ( H_f + H_b + h_f + h_b ) \Delta T \quad (II-2)$$

where

$H_f$  and  $H_b$  are the forced convection coefficient for the front and rear surfaces respectively.

$h_f$  and  $h_b$  are the coefficients of free convection for the front and rear surfaces

$\Delta T$  = effective temperature differential between the surface and the local ambient air

The effective coefficient of heat transfer for the front surface in a free convection mode is given in equation (II-3) for a module with a tilted angle of  $\theta$ . The relationship is valid for a tilt angle less than 70 degrees.

$$h_f = 1.519 ( \Delta T \cos \theta )^{1/3} \quad (II-3)$$

An approximate expression is also shown in equation (II-4) for the back surface of the module.

$$h_b = 0.48 ( \Delta T \sin \theta )^{1/3} + 0.83 ( \Delta T \cos \theta )^{1/3} \quad (II-4)$$

The coefficients are expression in  $W/m^2-C$  and the temperature difference is in degree Celsius.

Forced convective heat transfer for wind over a flat plate involves variables such as wind speed, wind direction, tilt angle and the interferences from local structures and terrain. For steady wind over a plate parallel to the air flow, the coefficient of heat transfer can be approximated by the linear relationship shown in equation (II-5)

$$H_f = H_b = 3.8 V \quad (II-5)$$

where  $V$  is the free-stream wind speed parallel to the module measured near the surface, m/s

Very few data are available for wind convection over a flat plate with different angles of approach. An experimental investigation of wind effect on PV modules was conducted in the JPL 25-ft solar simulator (Ref. 13). Based on the experimental results, a semi-empirical expression for forced convection coefficients (the sum of front and back surfaces in a rack-mounted situation) can be established as a product of wind speed and a directional distribution function D as shown in equation (II-6)

$$H_f + H_b = D(\omega) V \quad (\text{II-6})$$

where

D( $\omega$ ) is the distribution function for wind convection

V is the wind speed at module level measured in m/s

$\omega$  is the wind direction with 0 being the north and 90 being the east

Figure II-3 shows a plot of the function D( $\omega$ ), evaluated based on experimental data. Strictly speaking, the correlation is valid only for the specified test conditions: i.e., 30-degree tilt angle, open frame rack-mounted configuration and steady wind with zero elevation angle of approach. The correlation has been found to be quite satisfactory for other conditions as long as wind measurements are made close to the module. For many practical applications, it is further assumed that when the wind is coming from the rear (i.e.,  $\omega$  from -90 to 90 degrees) the module back surface is subjected to a uniform cooling with a constant  $H_b$ . Similarly, when the wind is coming from the fore-hemisphere ( $\omega$  from 90 to 270 degrees) the front surface has the constant coefficient of heat transfer. This assumption allows a decomposition of the distribution function into two components, one for the front surface and one for the rear surface.

### (3) Radiative Heat Transfer

Radiative heat loss from a tilted PV module is the net resultant energy balance between the infrared emission from the module surfaces and the incident IR from the sky and the ground.

$$Q_r = E - (B_f + G_f + B_b + G_b) \epsilon_m \quad (\text{II-8})$$

where

B and G are the energy incident to the module surfaces from the sky radiation and ground emission respectively. The subscripts designate the front and the rear surface of the module.

E is the infrared emission from the module surfaces. For most module designs the surface emittance values for the front and back surfaces are very close and can be represented by a single value  $\epsilon_m$ , the energy emission can be expressed as

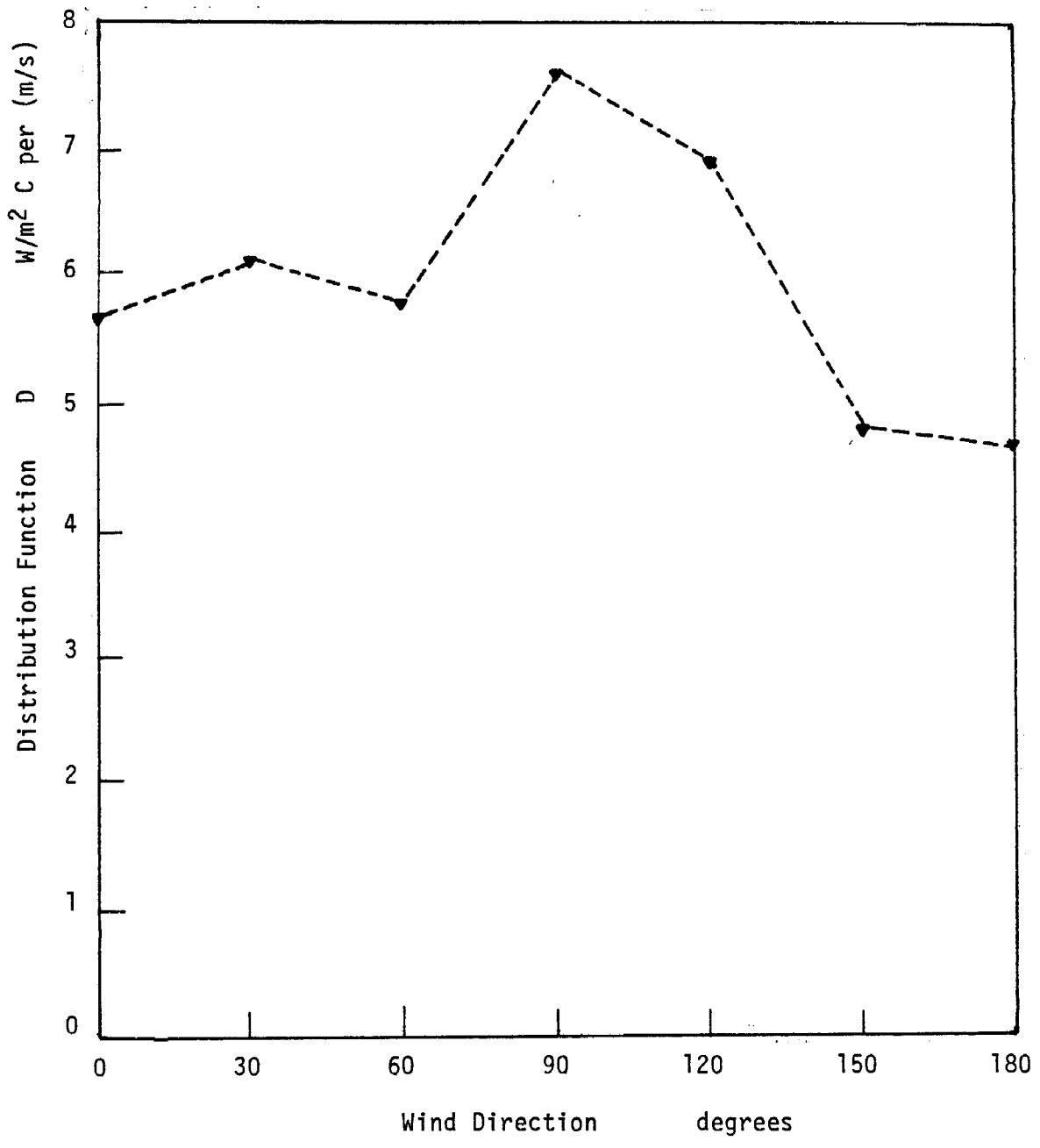


Figure II-3 Distribution Function D Versus Wind Direction

$$E = \epsilon_g A \sigma (T_f^4 + T_b^4) \quad (\text{II-9})$$

where

A module surface area

T<sub>f</sub> and T<sub>b</sub> are the front and back surface temperatures

σ = Stefan-Boltzmann constant, 5.6699x10<sup>-8</sup> W/m<sup>2</sup> K<sup>4</sup>

The effective ground emission to the front surface of a tilted flat plate can be expressed in equation (II-10) for a ground surface of uniform temperature T<sub>g</sub> and an effective emittance of ε<sub>g</sub> (Ref. 14):

$$G_f = \epsilon_g \sigma T_g^4 \text{Sin}^2(\theta/2) \quad (\text{II-10})$$

In a similar manner the ground emission to the module back surface can be approximatd by equation (II-11).

$$G_b = \epsilon_g \sigma T_g^4 \text{Cos}^2(\theta/2) \quad (\text{II-11})$$

However, for most flat-palte PV module applications, the ground temperature has to be separated into two distinct levels: one for those in the shadow and the other for the sunlit area. Furthermore, in many cases the view from the module to the ground is partially obstructed by other PV arrays.

At the earth surface, atmospheric radiation received on a tilted surface can be expressed as a sum of the flux from an isotropic source and one due to anisotropic radiation. Equation (II-12) shows the incident long-wave radiation on a tilted plane with an angle θ (Ref. 15,16).

$$B = L_d \text{Cos}^2(\theta/2) + f(\theta) \sigma T_a^4 \quad (\text{II-12})$$

where

L<sub>d</sub> is the isotropic sky radiation received on a horizontal surface

f(θ) is the anisotropic distribution function, whose value varies from 0 at zero degree to 0.027 at 30 degree and 0.065 at 60 degree tilt

T<sub>a</sub> is the ambient air temperature near the ground

## B. CORRELATING ANALYTICAL AND EXPERIMENTAL RESULTS:

### (1) Experimental Observation:

Figure II-4 illustrates a typical NOCT test data recording of cell temperature profiles (on day 307, 1982). During this period, the module was tilted to 56 degree from the horizon and the solar irradiance measured on the module surface was 970 W/m<sup>2</sup> at the beginning of the test, peaked to 1020 W/m<sup>2</sup> around noon then gradually declined to 870 W/m<sup>2</sup> at the end of the test period

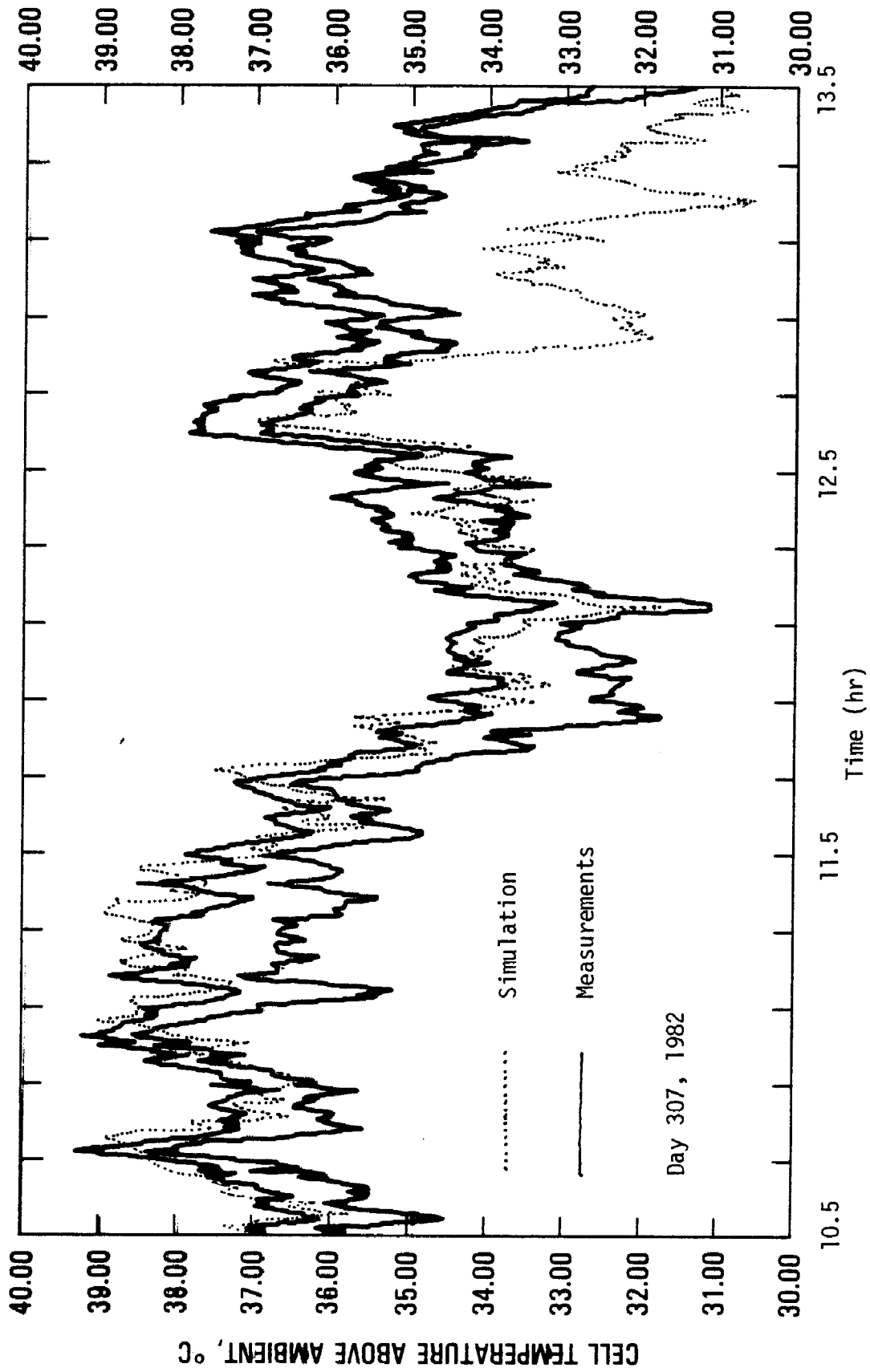


Fig. II-4 Representative Cell Temperature Profiles

around 2 pm. The ambient temperature increased steadily from 23 degree C to 26 degree C. The wind speed fluctuated in the range between 0.5 and 2.5 m/s while the wind directions were random.

The two solid lines in the figure represent the thermocouple readings of the two cells (located on the same module). These readings track each other but there exists a consistent temperature deviation of 1 to 2.5 degree C. The cyclic pattern of the temperature profiles does not correlate with either the solar irradiance variation or the ambient temperature changes. In fact, the minimum cell temperature occurred around noon when the solar irradiance was at its peak.

### (2) Transient Simulation:

Transient thermal simulation techniques have been employed in the past to assess the underlying factors governing the thermal performance of a module. Model parameters can be iterated to achieve a close approximation between the measured data and the simulated result. However, in many cases the model represents a under-determined mathematical system and the solutions are not unique.

The dotted line in Figure II-4 represents the results of a transient simulation. The thermal network model had been adjusted to achieve a close approximation with data obtained in previous tests. The resultant model was used here to simulate the module response to environmental changes. No further model adjustment was applied. It can be seen that excellent correlation exists in the first half of the experiment, between the simulated cell temperature and one of the measured profile. The simulated profiles display the same cyclic pattern and the same high frequency fluctuations as the measured profiles, one can conclude that these fluctuations are not measurement errors but are the dynamic response to wind variation. The rate of temperature change can be as high as a few degrees per minute inspite of the damping effect by the module thermal inertia. In the second half of the experiment, the similarity in the cyclic pattern and the high frequency fluctuation still exists between the simulated and the actual temperature profiles. However, the simulated temperature becomes noticeably lower than the measured level. It is as if certain supplementary afternoon heating to the module was ifgnored in the analytical mode.

### (3) Assessment of Uncertainties:

The discrepancies observed in Figure II-4 are fairly typical. Cell temperature differentials have been commonly observed for the cells on the same module. Trends in temperature variations are usually different in the afternoon from those recorded in the morning.

In a no-load, open-circuit thermal testing conditions, such as the NOCT testing, temperature gradient along a single module should be negligible. This is observed for about half of the test cases. The two cell temperature readings on these modules are usually within fractions of one degree. However, temperature difference up to 2.5 degree C between two cells (on the same module) was also consistently observed for many other modules.

One possible source for this discrepancy is thermocouple measurement error. It was detected in the past that some of the thermocouples were not mounted on the silicon surface, due to installation error or caused by a detachment. Consequently, the reading does not reflect the cell temperature (usually shows a lower value than actual reading). It is also possibility to have a separation of the adhesive bond developed between the cell (or part of the cell) and the substrate. This may be caused by material delamination or caused by the thermocouple installation process. In either cases the local thermal resistance between the cell and the substrate will be significantly increased. Consequently, during solar heating this particular cell will have a testing temperature higher than other cells, and the corresponding substrate temperature would be lower than normal.

Another possible cause of the cell temperature deviation is the local wind effects. Air ventilation to the back surface of the module have been observed to cause large temperature gradient in a large size array. If the module mounting configuration provides significant wind interference such that part of the module is subjected to a different wind cooling than other parts, then appreciable temperature gradient can be developed.

The fact that analytical simulations are capable of tracking the high frequency temperature fluctuations suggests that the heat transfer correlations for forced convection due to wind variations is adequate. On the other hand, the AM-PM discrepancy clearly demonstrated that the established method does not completely account for all environmental influences. In the established test procedure, only the major meteorological quantities are monitored. These include solar irradiance, ambient temperature and wind conditions. The effects of secondary environmental factors are either ignored or being modeled with over-simplified approximations. For example, Inaccurate representation could lead to significant errors in sky radiation effects. The solar energy reflected by the ground to the back surface of the module is traditionally ignored. Infrared emission from the ground has been assumed to be emitted from a uniform ground having the same temperature as that of the ambient air.

The present investigation is concentrated on reducing these uncertainties. A series of special experiments is designed to establish an improve test procedure and to provide more reliable heat transfer correlations for these secondary environmental factors.

## SECTION III

### EXPERIMENTAL INVESTIGATION

The simple assessment presented in the last section suggests that the deficiency in the understanding of module thermal performance was caused either by experimental errors or by crude modelling of the effects of secondary environmental factors, including the ground reflection/emission and the sky radiation characteristics. A special series of experiments was designed to calibrate both the experimental measurements and the heat transfer correlations commonly used in the analysis. An open-frame, rack mounted Motorola module was selected as the testbed. Environmental parameters are carefully monitored. Redundant measurements were also made to provide secondary references such that experimental errors can be minimized. Additional instruments were also installed to monitor ground reflection/emission and sky radiation. The series of experiments was conducted in three consecutive phases from Nov. 18, 1983 until January 13, 1984. The first phase was for instrumentation set up and sensor calibrations. Sky temperature radiation was investigated and compared to existing heat transfer correlations in phase 2 between November 28 and December 5, 1983. In the final verification phase, four sets of experiments were conducted under clear sky conditions between January 5 and January 13, 1984.

#### A. EXPERIMENTAL SETUP

##### (1) Test Site and Environmental Conditions:

The thermal test area for photovoltaic modules at JPL is located on the roof top of building 248. Figure III-1 shows an overview of the test area. During the test periods (usually three hours each day) thirty channels of test signals were transmitted, at a rate of every 15 seconds, to a Hewlett Packard computer residing in the adjacent building.

##### (a) Local Wind Condition:

Although the correlation between wind speed and forced convection heat transfer has been established and verified, however the variation in wind conditions is still considered to be the most difficult factor to handle in analyzing module thermal responses. This is because ground and structural interference can drastically alter the local wind conditions within a short distance. At the test site, wind conditions are monitored by two Mark III Vector Van sensors, one on each side of the east and west edges. Figure III-2 shows a typical wind speed profile measured with the west anemometer. Wind direction at the test site appears to be a random function versus time. Local turbulence is illustrated by the in-coherency displayed by the wind direction measurements, shown in Figure III-3-a and b, made by the two anemometers separated only about 12 meters apart. Because of the vastly changing local wind characteristics, one has to make certain the the measured wind condition indeed represent the true local effective wind conditions at the test hardware.



Fig. III-1 Overview of JPL Thermal Test Site

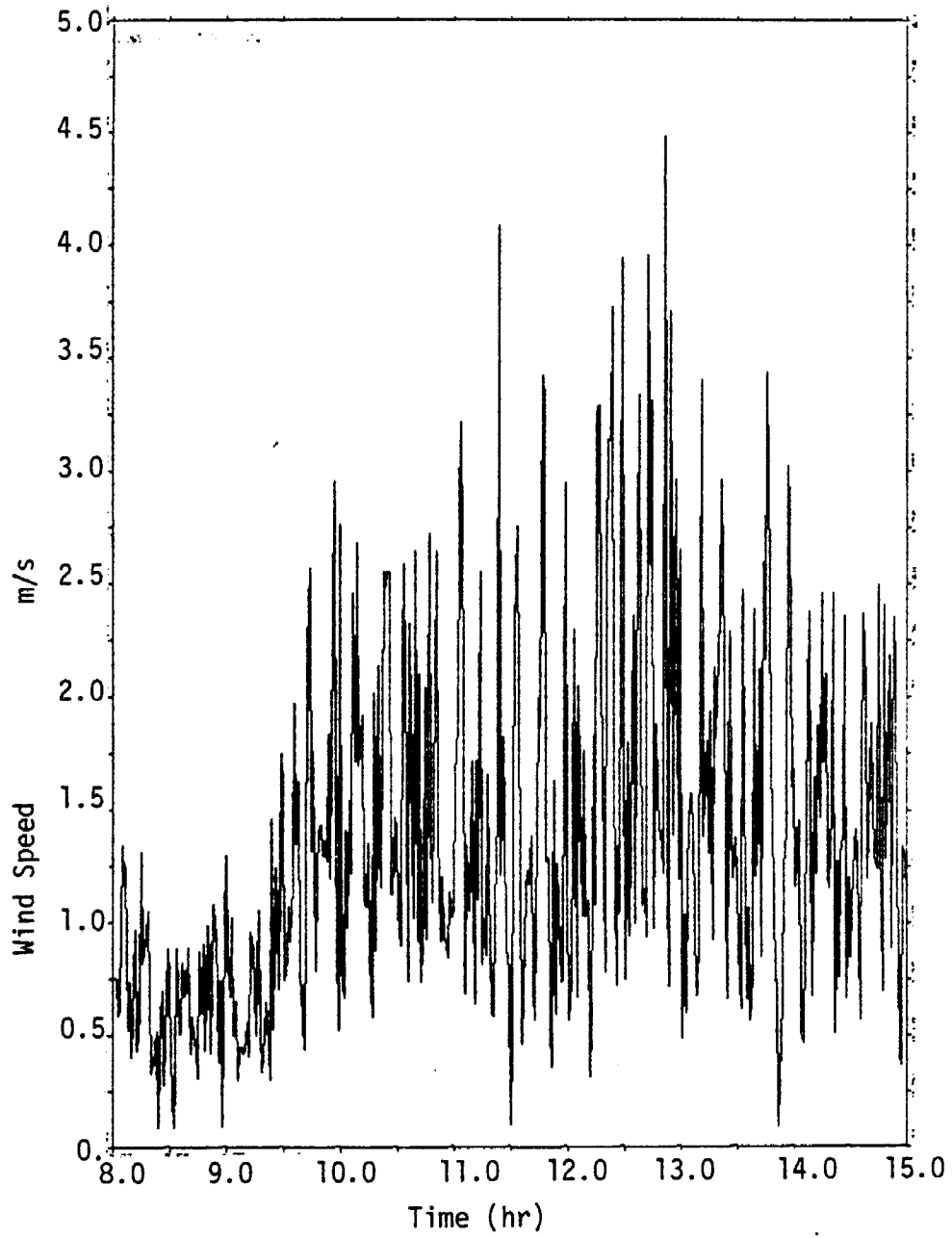


Fig. III-2 Representative Wind Speed Variations at the Test Site

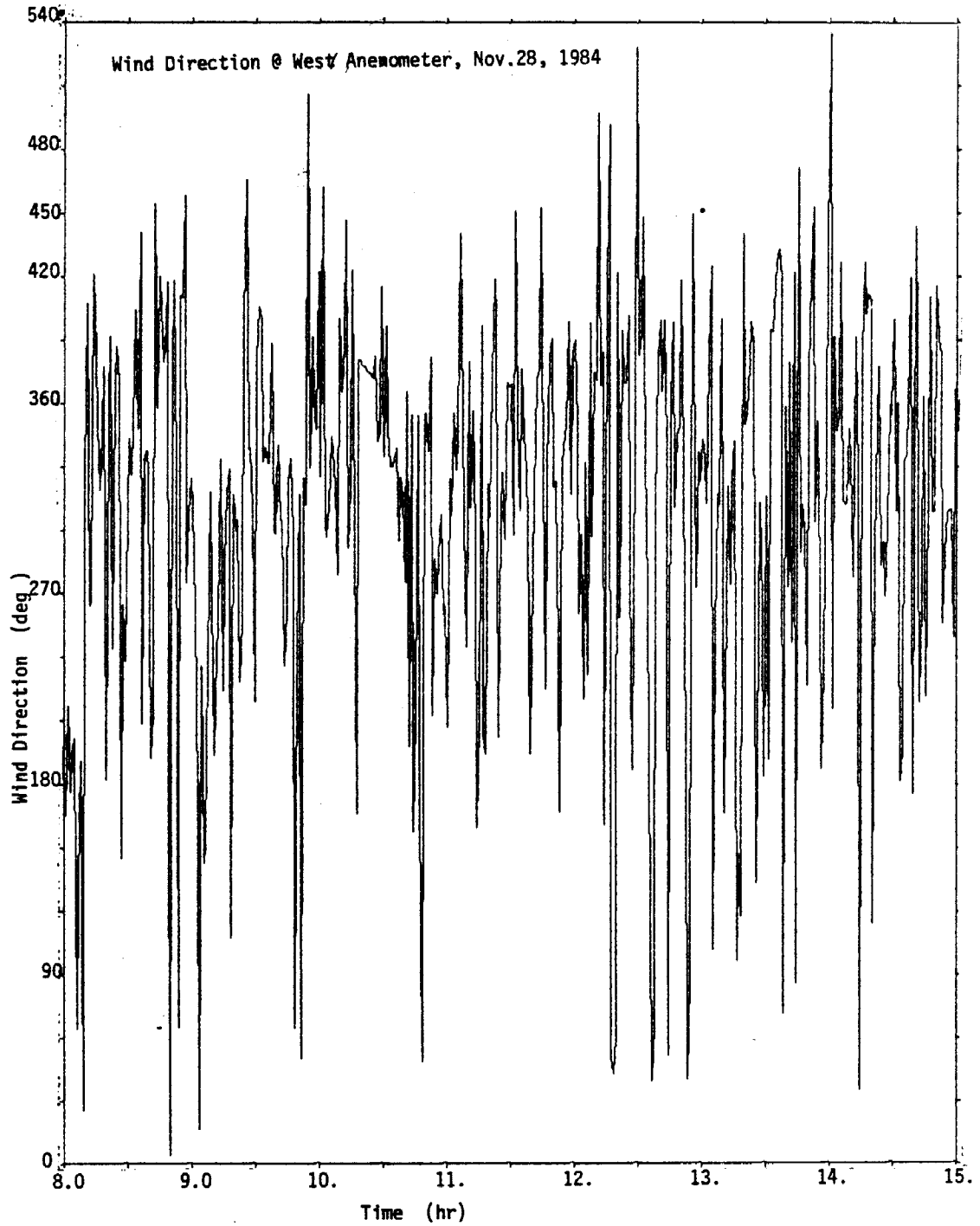


Fig. III-3-a Typical Wind Direction Variations at the Test Site (West Anemometer)

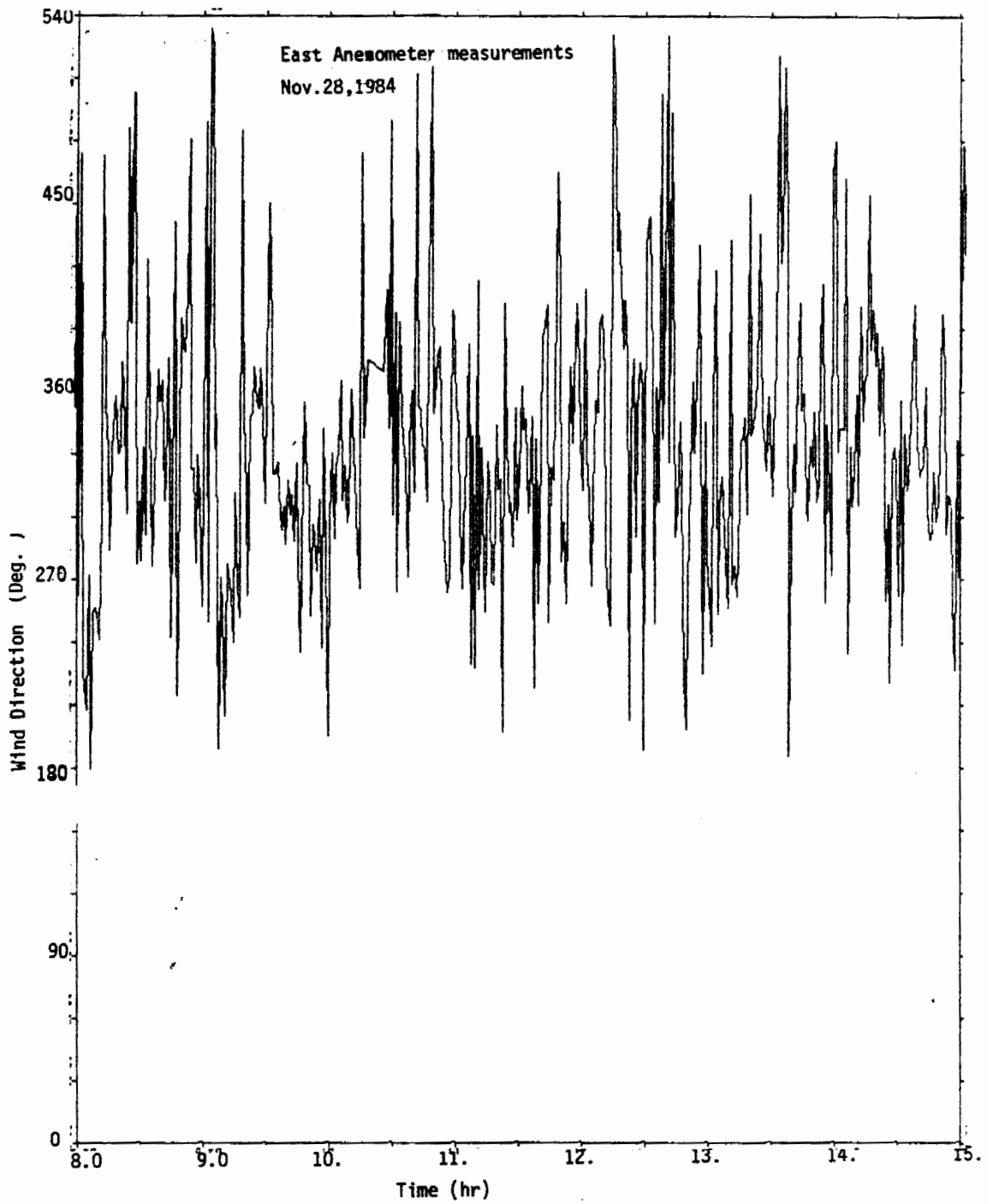


Fig. III-3-b Typical Wind Direction Variations at the Test Site  
(East Anemometer)

(b) Solar irradiance and Ground Reflection:

Two Epply pyranometers, one PSP and one B + W types, were mounted on the plane of the modules. Both instruments were calibrated, on December 8, 1983, for various angles of incidence, against a reference MARK VII pyranometers. Significant errors appear to have developed for both instruments since their last calibrations. The PSP was found to measure irradiance about 3 % too low at zero degree incidence. The error increases to 7.8 % at a 56 degree angle of incidence. The B + W, on the other hand, measures irradiance levels 5 to 9.2% too high. In all past data reductions at JPL, the PSP readings were used as the primary measurements of solar irradiance at the test site. This practice is continued in the present study.

In addition to the two pyranometers, standard solar cells, mounted on reference plates, were also used to monitor the solar irradiance. The relationship between the cell reading and the PSP irradiance values is fairly linear. The relationship shown in Figure III-4 can be approximated by a straight line. One of the standard cell sets was used to monitor the irradiance reflected from the ground to the back surface. Figure III-5 compares the direct incident solar irradiance received at the front surface to the reflected flux at the back surface for a plate tilted at 30 degrees from horizon. It can be seen that ground reflection contributes additional 10 to 12 % solar flux to the module. Although most module designs consists of a light colored (low absorptance) back surface, the additional solar flux caused by ground reflection should still provide about 3% additional heating, which has been ignored in previous analyses or NOCT data evaluations.

(3) Ambient Temperature:

Ambient temperature is monitored with four thermocouples. A shielded thermocouple suspended behind the module serves as the primary sensor. A un-shielded 'pig-tailed' thermocouple, protruding out near the center of the module, is used to include environmental infrared radiation. Two 'aspirated' air temperature sensors (model 840 series, Meteorology Research INC.), measuring temperatures with air vented with small motor fans into the thermocouple cavities, are each located underneath a wind sensor.

All four temperature sensors for monitoring ambient air temperatures have readings within fractions of one degree during night measurements. However, during sun-lit period significant differences can be observed. Figure III-6 shows a typical comparison of the ambient temperature recordings. The shielded thermocouple reading, which is considered to be an accurate recording of the local air temperature, is represented by curve b. The un-shielded thermocouple ( the pigtail as represented by curve a) recorded a temperature level 2 to 3 degrees higher because of the additional infrared heating. The two aspirated sensors measured temperatures about 0.5 to 1 degree cooler than the shielded one. This may be due to the factor that the locations (at the stem of the anemometer) are having an elevation higher than the module back surface. Slight delays in temperature responses were often observed for the two 'asperated' thermocouples. These are probably caused by the additional thermal mass of the anemometer stems.

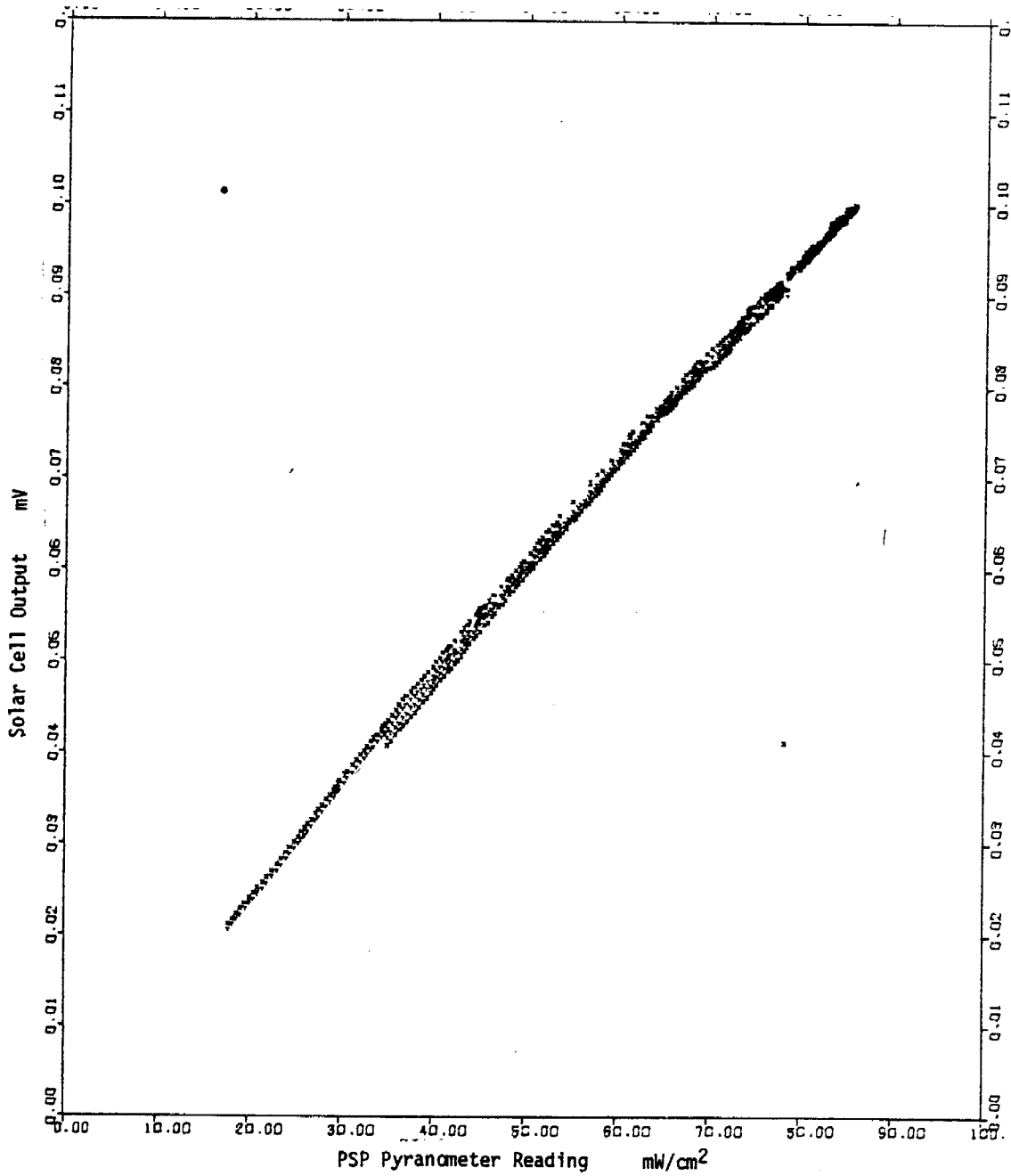


Fig. III-4 Correlations between Pyranometer Readings and Solar Cell Measurements

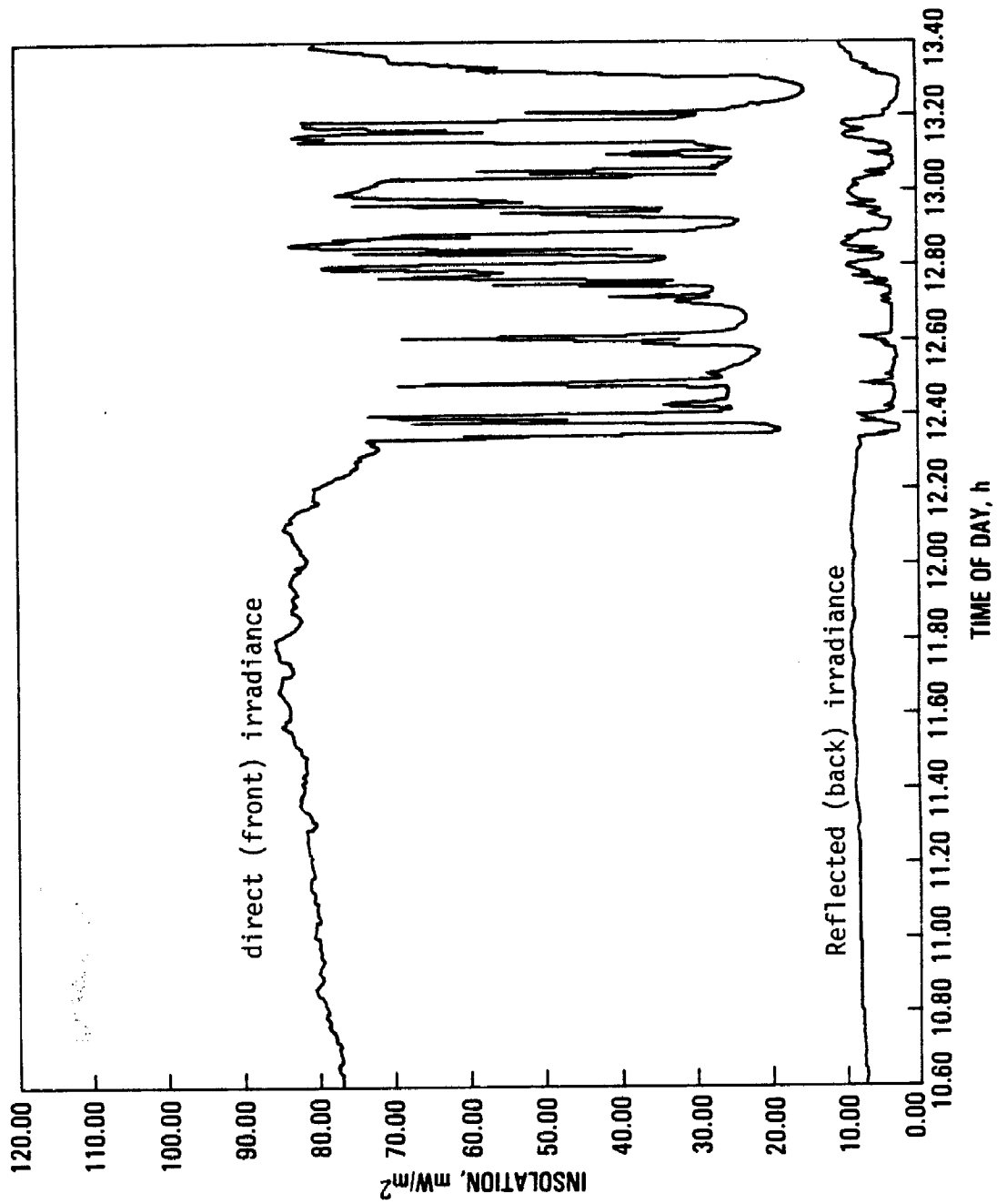


Fig. III-5 Comparisons of Direct (Front) Solar Irradiance and Ground Reflection

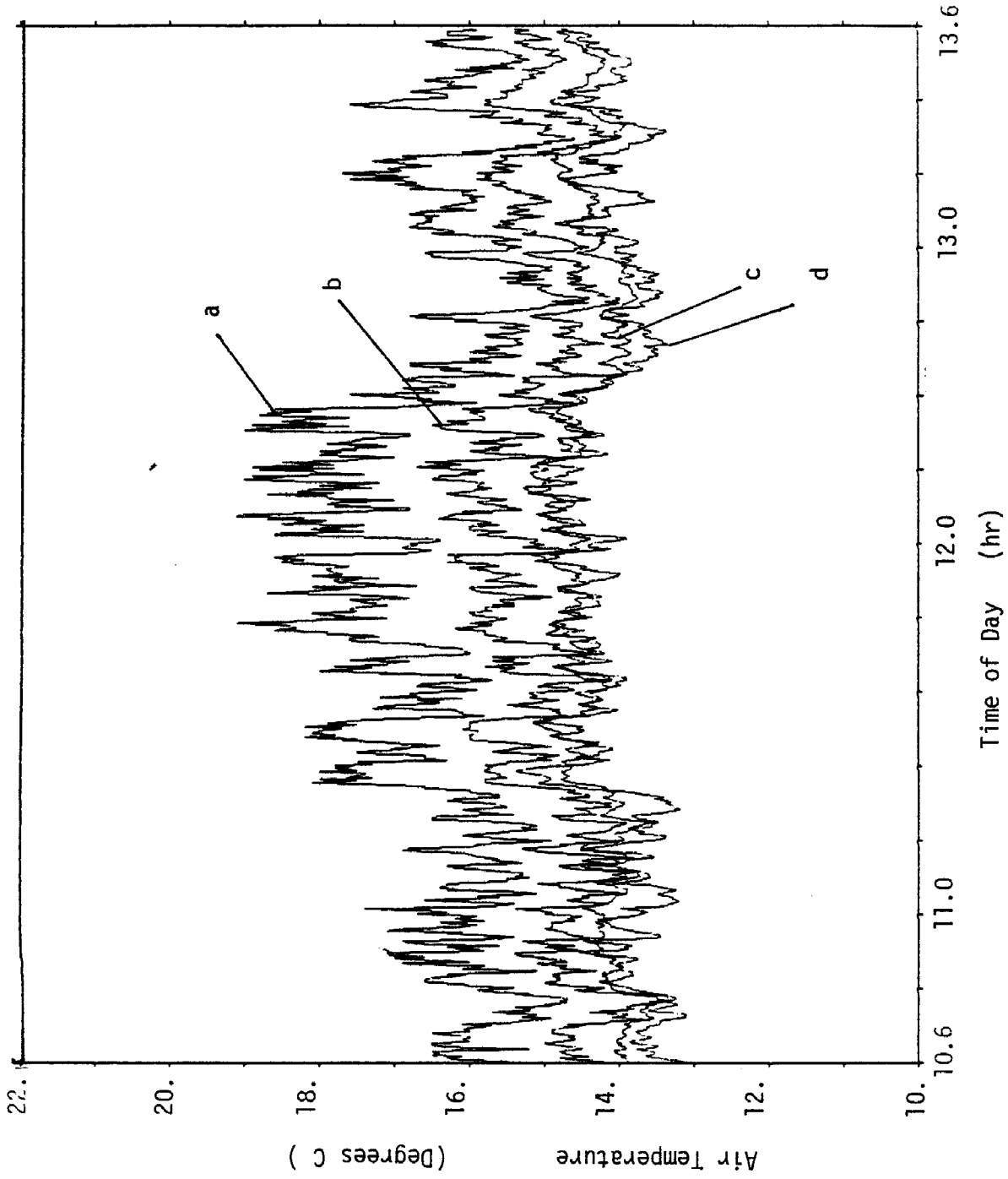


Fig. III-6 Ambient Temperature Profiles

## (2) Test Hardware and Sensor Calibrations:

A Motorola module (Model MSP43E40B, test item ID BROH-5075) and three reference plates are the test hardware considered in this study. The reference plates were specially constructed as auxiliary diagnostic tools. They are made with 12-1/4 by 19 by 3/16-in hard aluminum plates (California Chassis Company Cat. No. PWHA-10 P4086-7). The front side of the plate is painted with Bostic Flat black No. 463-3-8 Temperature Control Paint. The optical properties are assessed to be 0.92 for effective solar absorptance and 0.86 for surface emittance. The back surface and the edges are coated with Bostic Thermoflect Gloss White No.443-1-500 TRS paint. The solar absorptance is 0.2 and the IR emittance is 0.85. Two thermocouples are installed on the plate to monitor the plate temperature. Two square PV cells are installed on the front (black painted) surface of each plate as auxiliary sensors for irradiance measurements.

Two of the reference plates were mounted on the same frame, with the black surfaces facing south, placed next to the east edge of the Motorola module. One of these reference plates has been in the test site for six months, while the other was just taken out of the shelf. The two black painted surfaces looked distinctly different due to the weathering effect. The third reference plate was mounted, in an inverted position (with the black surface toward north), on a separated frame to the west of the Motorola module. This arrangement allows the solar cells mounted on the back surface to monitor the reflected solar irradiance to the back of the module. The front side of this frame was covered with a thick layer of white insulation to isolate the plate from direct solar flux and sky radiation.

All test hardware were situated near the west anemometer. Spacing is left between frames to allow air movement such that wind interference can be reduced and the local wind conditions would not be too different from that measured by the anemometer. This is a practice quite contrary to the standard NOCT test procedure where modules are butt up against each other to form a continuous array and additional plates are placed around the rim of the rack to minimize edge effects.

The cell temperatures are monitored with 36-gauge chromel-constantan thermocouples installed on the back surface of the silicon cell itself. This was done by physically cutting away 1/2-inch holes on the substrate underneath the cell. The thermocouple junction is soldered on the silicon surface. The hole is then filled by a 1/2-inch button with similar epoxy material as the substrate. In order to ensure the validity of the cell temperature measurement, two separated cells are monitored. In this special series of experiment each cell has two independent thermocouples installed on the back silicon surface, providing a total of 4 cell temperature measurements per module. Module back surface temperature was also monitored through two 26-gauge thermocouples installed on the rear surface of the module near the locations where cell temperatures were measured.

Thermocouple calibration was performed in two steps. The first step is to verify the thermocouple measurements in a room temperature environment. The test hardware and related thermal sensors are situated inside a room and stabilized for 24 hours before thermocouple readings were taken. The result shows that all the thermal sensor reading during the calibration period are

within 0.1 degree Celsius of the measured room temperature.

The second series of calibration was performed in a three-day continuous testing. The data recording started on Nov. 18, 1983 around 4 p.m. The two reference plates show close temperature ranges at night. However, the old plate temperature is slightly ( 1 degree C ) lower than the new one. This could be caused by absorptance degradation ( a visible difference can be detected ) or it could be caused by the altitute difference since the new plate was mounted on top. The inverted reference plate ,on the other hand, was significantly cooler than the black plates in day time periods and was slightly warmer at night. This is attributed to the blockage of solar and sky radiation at its front surface.

The Thermocouple calibration process was terminated at this point. In the following days, the module and the black reference plates were moved around and instrumentation was added to prepare for the second phase of the experiment. The four thermocouples ( two on each cells) on the cells have been recording temperatures within 0.5 degrees for all test cases. The thermocouples on the reference plates display the same situation, showing no appreciable difference caused by paint degradation or plate position.

#### (B) GROUND EMISSION:

Ground temperatures are measured with three individual thermocouples: one located approximately 10 ft in front of the module, one underneath the module and one located about 10 ft away from the module's rear surface. Figure III-7 shows typical temperature profiles recorded by these three ground thermocouples. Curve (a) shows the ground temperature of the sunlit area to the front of the test rack. Curve (c) shows the temperature of the shaded area underneath the test rack. Curve (b) display the ground temperature of an area that is shaded occasionally. Because of the sun's relative position, the complex shadow pattern created by the sparsely spaced modules varies continously with time.

#### (C) SKY RADIATION

Accurate accounting of the sky radiation effect to the module thermal performance is a complex process. The downward atmospheric radiation flux density is composed of partial fluxes of water vapor, carbon dioxide, ozone and aerosol. The magnitude varies from 200 W/m<sup>2</sup> in a clear winter night to a level above 400 W/m<sup>2</sup> in a cloudy summer day. There are basically three different ways to determine the amount of atmospheric radiation: (1) monitor with a pyrometer or a radiometer for angular and spectral measurement of thermal fluxes, (2) computation using detailed profiles of atmospheric constituents and radiative properties and (3) assessing with empirical formulae based on environmental parameters measured near the ground. The third method was adopted in the present study for the reason of simplicity. Many independent research papers have been published in the literature since 1915 after A. Angstrom suggested the well known formula for predicting the sky radiation quantity for a clear sky. Most of the correlations are based on the observation that atmospheric downward radiation correlates well with the ambient air temperature and humidity measured near the ground level for a cloudless sky.

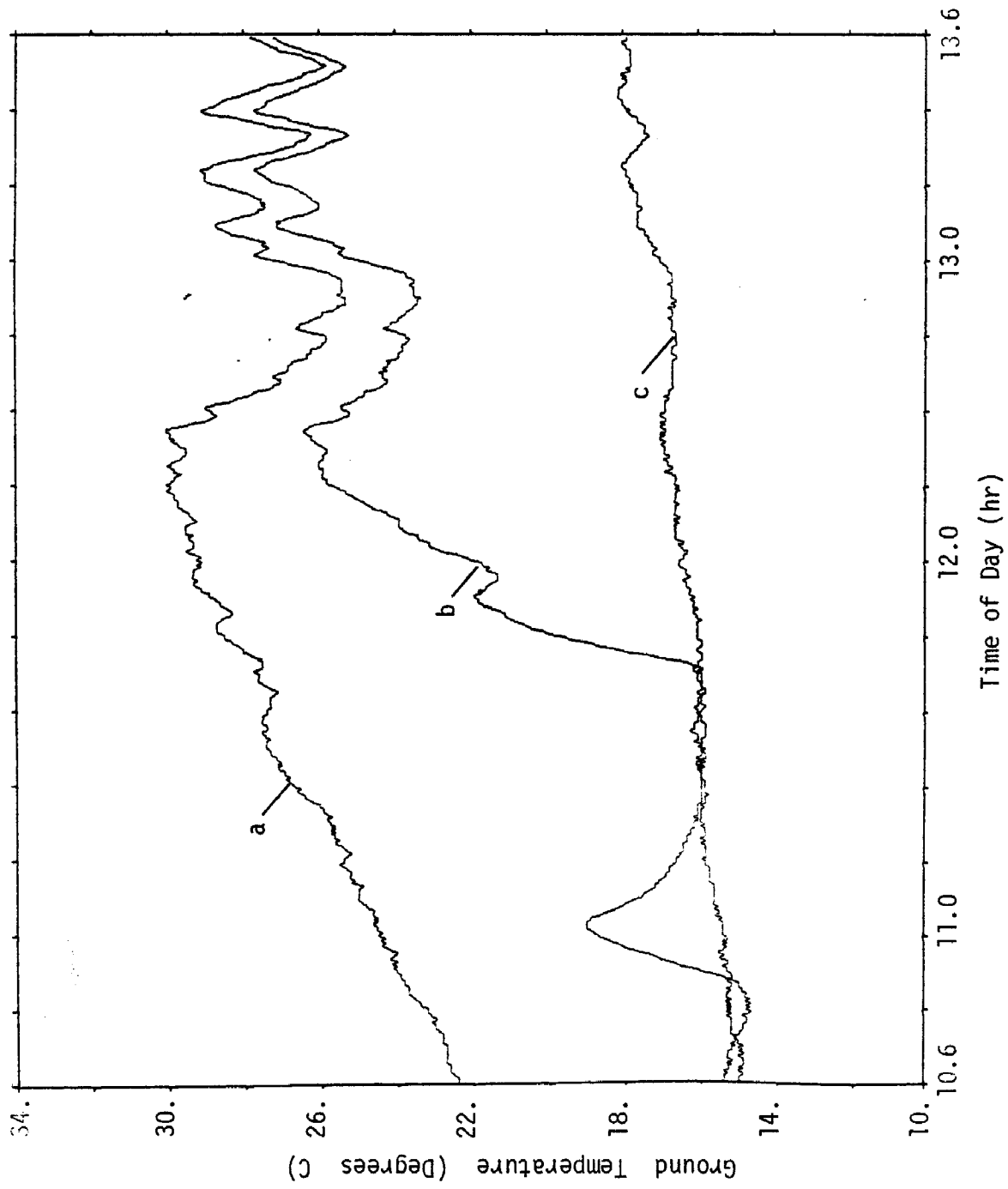


Fig. III-7 Ground Temperature Distributions

The variation in sky radiation has been considered as a significant factor contributing to the uncertainty level of PV module thermal evaluation. It is one of the major objectives of this study to calibrate this particular source of uncertainty. The approach can be separated in three stages: (1) to perform a thorough literature survey of the empirical relationship developed over the years, (2) to design and conduct a special calibration experiment at the test site and (3) to compare the experimental results with the predictions made by these formulae. The equation that provides the closest approximation can be selected as the basic model for thermal simulation analysis.

Isotropic sky radiation received on a horizontal surfaces,  $L_d$ , can be represented by many different expressions. The classical equation is expressed in terms of the so called 'effective atmospheric emissivity',  $\epsilon_a$ , and the ambient air temperature,  $T_a$ .

$$\epsilon_a = L_d / T_a^4 \quad (\text{III-1})$$

A number of equations have been proposed to correlate the atmospheric emissivity with basic environmental parameters including ambient air temperature and humidity. Some of the better known empirical relationships are listed as follows:

$$\epsilon_a = 0.82 - 0.25 (10)^{-0.126 \gamma} \quad (\text{III-2})$$

This is the well known relationship by Angstrom (Ref 17).  $G$  is the pressure of water vapor measured at an elevation of 1.5 m to 2 m. The coefficients were evaluated by Boltz and Falkenberg (Ref.18). Another well known expression was proposed by Brunt (Ref.19) as shown in equation (III-3). Stanley and Jurica (Ref.19) modified the relationship as shown in equation (III-4)

$$\epsilon_a = 0.45 + 0.056 (\gamma)^{0.5} \quad ; \delta \text{ in millibars}$$

or

$$\epsilon_a = 0.60 + 0.042 (\gamma)^{0.5} \quad (\text{III-3})$$

$$\epsilon_a = 0.67 (\gamma)^{0.08} \quad (\text{III-4})$$

Berdahl (Ref.20) established a correlation in terms of the ambient dew point temperature,  $T_{dp}$  (equation III-5) and Centeno (Ref.21) proposed an expression to estimate the effective atmospheric emissivity in terms of the local altitude,  $Z$  (in km), ambient temperature,  $T_a$ , and relative humidity, as shown in equation (III-6)

$$\epsilon_a = 0.741 + 0.0062 T_{dp} \quad (\text{III-5})$$

$$\epsilon_a = f(Z) f(T) f(\gamma) \quad (\text{III-6})$$

where

$$f(Z) = 5.7723 + 0.9555 (0.6017)^Z \times 10^{-4}$$

$$f(T) = T_a^{1.893}$$

$$f(\gamma) = \gamma_r^{0.0665}$$

In many recent investigations the atmospheric radiation is estimated by means of ambient temperature alone, without reference to atmospheric humidity. IDso and Jackson (Ref.22) based on their experimental observation suggested that the atmospheric emissivity has a minimum at 0° C, and increases symmetrically at higher and lower temperatures as shown in equation (III-7)

$$\epsilon_a = 1. - 0.261 \text{EXP}(-0.000777 \times (273. - T_a)^2) \quad (\text{III-7})$$

Unsworth (Ref.23) proposed the following expressions shown in equations (III-8) and (III-9)

$$L_d = 213 + 5.5 T_a \quad (\text{III-8})$$

or

$$L_d = 1.06 T_a^4 - 119. \quad (\text{III-9})$$

In many engineering applications atmospheric radiation is expressed in terms of the effective sky temperature,  $T_{\text{sky}}$ , as shown in equation (III-10).

$$L_d = \sigma T_{\text{sky}}^4 \quad (\text{III-10})$$

with

$$T_{\text{sky}} = T_a - \delta \quad (\text{III-11}) \text{ (Ref.24)}$$

$\delta$  is the temperature depressor and was suggested to have a value around 6 degree C (Ref.24). However, during the winter season the value may have to be adjusted to be about 20 degrees according to Reference 25. Equations (III-12) and (III-13) are the more recent engineering correlations for estimations of sky temperatures.

$$T_{\text{sky}} = 0.914 T_a \quad (\text{III-12}) \text{ (Ref. 26)}$$

$$T_{\text{sky}} = 0.0552 T_a^{1.5} \quad (\text{III-13}) \text{ (Ref. 27)}$$

The temperatures are expressed in absolute degrees (Kelvin). These relationships are simple and easy to use. However it could be grossly in error in many instances (as was discussed in References 28,29,30). The IR sky temperature is a complex function of cloudiness, humidity, surface temperature and geographical location.

Because past investigations indicated that atmospheric downward radiation correlated well with the air temperature and air humidity measured near the ground (2-meter elevation) for cloudless sky, a hygrometer was installed, at the test site, about 2-meter above ground to measure the dew point temperature. The hygrometer output is expressed in milli-volts. The instrument used is Model 2000, probe type M22R, Serial No. 13461-PR and was calibrated on Oct. 25, 1983. The output was converted into dew point temperature and then transformed into partial vapor pressure.

All the correlations listed above are for cloudless sky only. For cloudy skies the situation becomes much more complicated. This is primarily because that the cloud sheet absorbs and radiates as a black body while higher clouds are usually colder than low clouds. Furthermore the measure of cloudiness is non-quantitative and not precise. There are, nevertheless, a number of expressions established in attempting to estimate the effective atmospheric emissivity of a cloudy sky. For example, Centeno (Ref.21) used a quantity defined as nebulosity,  $n$ , to index the night sky condition.  $n=0$  is a lipid sky and  $n=1$  is for complete overcast. There are additional 22 levels of nebulosity between 0 and 1. The effective atmospheric emissivity are expressed as

$$\epsilon_c = \epsilon_0 + n(\epsilon_1 - \epsilon_0) \quad (\text{III-14})$$

where  $\epsilon_0$  is the atmospheric emissivity of a clear sky and  $\epsilon_1$  is that for a complete overcast sky.

Unsworth (Ref. 23) proposed a similar expression

$$\epsilon_c = (1 - 0.84 C_n) \epsilon_0 + 0.84 C_n$$

where  $C_n$  is the cloudiness factor

Because clouds is a strong emitter, the effective atmospheric emission can be significantly altered by the cloud conditions. A Raytek infrared thermometer was used to detect the presence of cloud by measuring the radiance between 8 to 10 microns. The measurement indicates, on a gross scale, the water content in the cloud layers. Although the method is very crude, nevertheless, the simple reading correspond very well with visual observations. In a cloudless day the reading would be -50 or out of scale. On a cloudy day the reading can be as high as 10 to 15 on the scale. In other words, sufficient resolution can be obtained to provide a relative index in characterizing the cloud condition.

The calibration experiments for atmospheric radiation were performed with the two reference plates described earlier. The front of one of the plates was covered with thick thermal insulation material to inhibit radiative heat transfer between the front surface and the environment, while the other plate was allow to radiate to the surrounding. Energy balance on each plate was computed based on the temperature measurements and environmental parameters. The contribution of atmospheric radiation can be calculated. The experiments were typically conducted between midnight and 3 am such that

the influence of transient ground emission variations can be minimized. Figure III-8 shows the sky radiation level evaluated experimentally on day 333, 1983 between midnight and 3 a.m. The sky conditions had been very clear and the Raytak reading was out of the scale. Ten different semi-empirical correlations were used to estimate the atmospheric radiation level for the calibration periods based on corresponding ambient temperature and humidity measurements. For the calibration period of these cloudless nights, equation (III-5) was found to provide the best correlations between the measured quantity and predicted values. The solidlines in Figure (III-8) shows the two limiting sky radiation levels: a cloudless sky,  $n=0$ , and a completely overcast condition,  $n=1$ . Figure III-9 shows the experimental data obtained for a cloudy sky. The results show that the empirical equation (III-5) can adequately bracketed the sky radiation levels. However, it is extremely difficult, if not impossible, to accurately differentiate the degree of cloudiness. Consequently, in the remaining part of the test period only the data obtained in cloudless conditions were utilized in the present study.

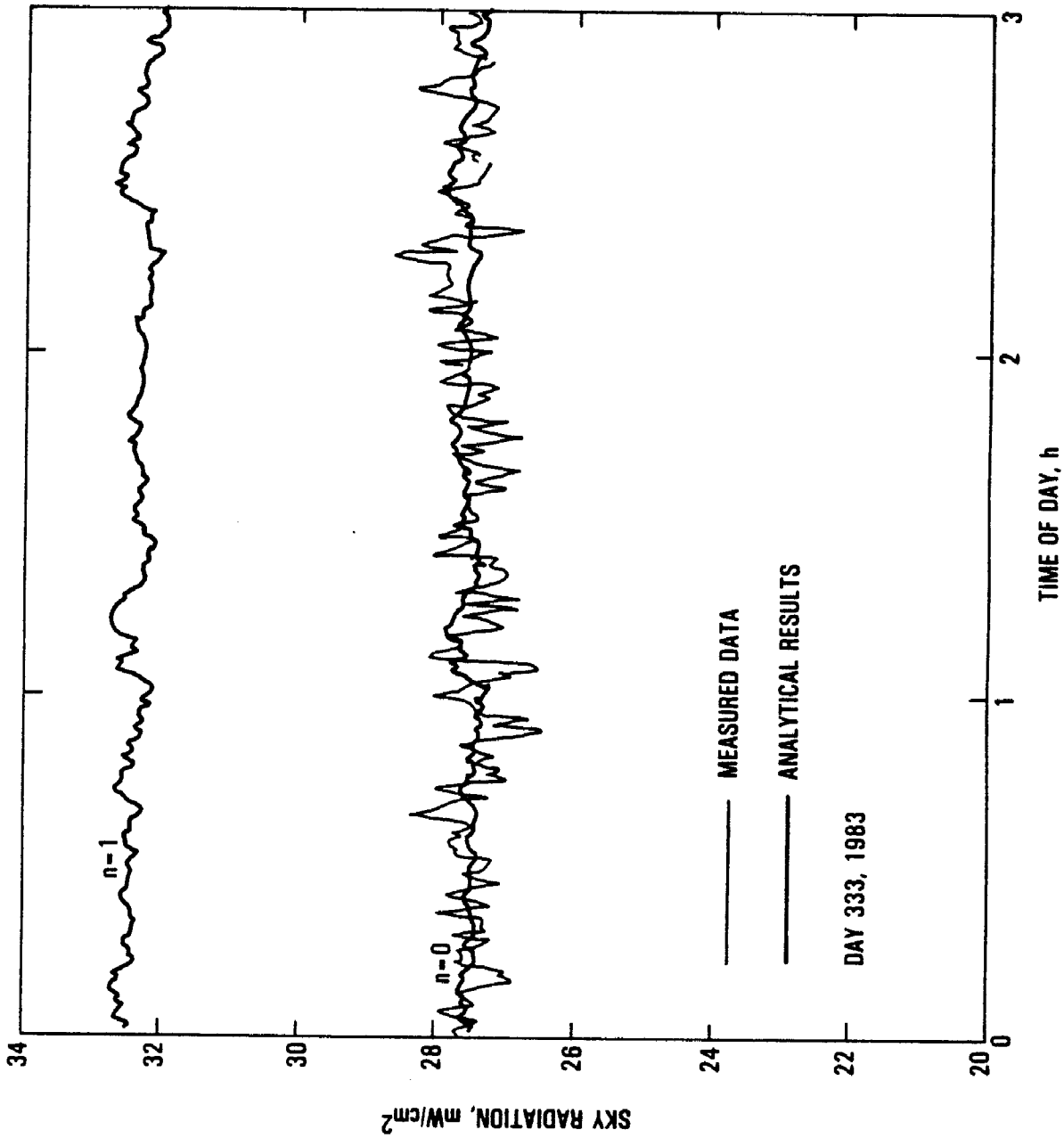


Fig. III-8 Atmospheric Radiation from a Cloudless Sky

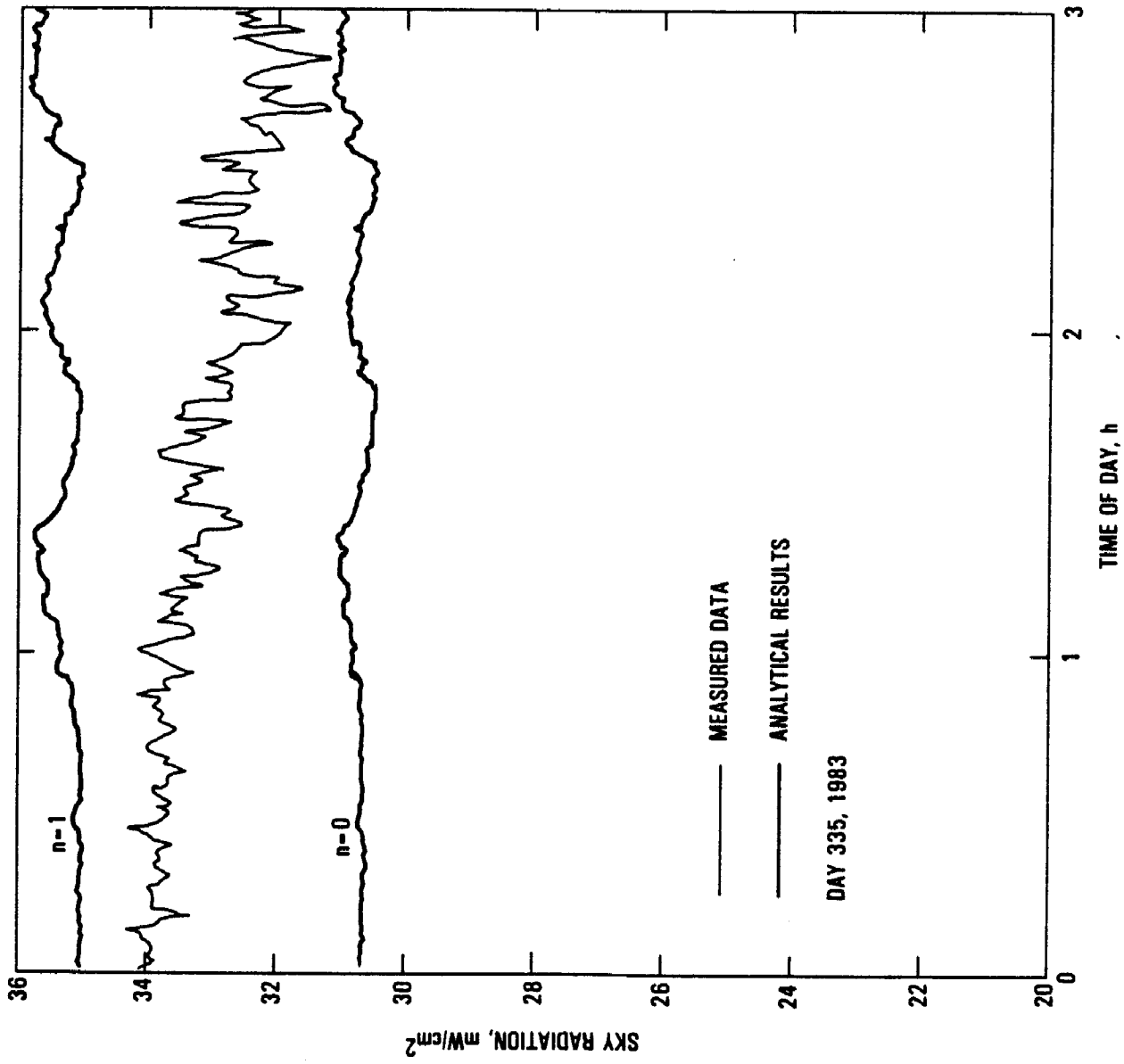


Fig. III-9 Atmospheric Radiation from a Cloudy Sky

## SECTION IV

### MODEL VERIFICATION AND DISCUSSION

#### A. TRANSIENT SIMULATION:

Thermal simulation techniques have been used in the past, as a tool, to understand the thermal behavior of photovoltaic modules. It was also used in assessing the effects of pertinent design parameters and was employed for verifying the accuracy of established thermal models. In this type of analysis, the fundamental step is to construct an analytical model. Transient simulations are then performed and the results are compared to experimental data. An unknown parameter in the model can be iterated until the prediction matches the experimental data. This adjustment process is very effective in determining the range and the sensitivity of the parameter. After the completion of the adjustment process, the analytical thermal model is considered to be corrected. A different and independent set of transient simulation can be performed using the ~~uncorrected~~ thermal model under specified boundary conditions. Corresponding experimental data are used to verify the model. It should be noted however, because there are many parameters governing the thermal performance of a module, too often one can match experimental results by over-compensating certain parameters to account for the effects of other parameters that were under-estimated. In order to improve the validity of the analysis, the models should be required to match the data obtained from multiple independent experiments. In the present study the thermal network models were first developed based on measured thermophysical properties and established heat transfer correlations. Extensive testing data were used to refine the heat transfer correlations. The final validation of the resultant thermal model was performed by comparing experimental temperature profiles with transient temperature simulations in an independent series of experiments. Analytical results were simulated using measured environmental parameters and no further parameter adjustment was performed. Because of the difficulty and non-preciseness of describing the degrees of cloudiness, all verifications were conducted under cloudless conditions. The sky radiation component was assessed using equations (II-12) and (III-5). Ground emission was based on measured ground temperatures. The ground surface in front of the test hardware was not shaded at all. The area facing the module back has a complex shadow pattern which varies with the time of a day. In the model it was assumed that 40% of the ground area was in the shade. Solar irradiance for both the front and the back surfaces were monitored. Ambient air temperature is measured with the shielded thermocouple. Wind conditions was monitored by the west anemometer which is approximately 6-ft away from the test hardware packages. All data were recorded every 15 seconds.

The thermal model consists of 14 nodes and the transient simulation was computed with a time step of 0.1 second. It should be pointed out, in the verification phase all the parameters are pre-determined and no parameter adjustment was performed to match the result. Figures IV-1 and IV-2 show two representative results. The dotted lines represent experimental measurements while the solid lines are analytical simulations. It can be seen that the simulations represent very close approximation in all cases. The simulated temperatures are slightly lower than the measured values and the root mean square error is less than 1 degree C for all four test cases.

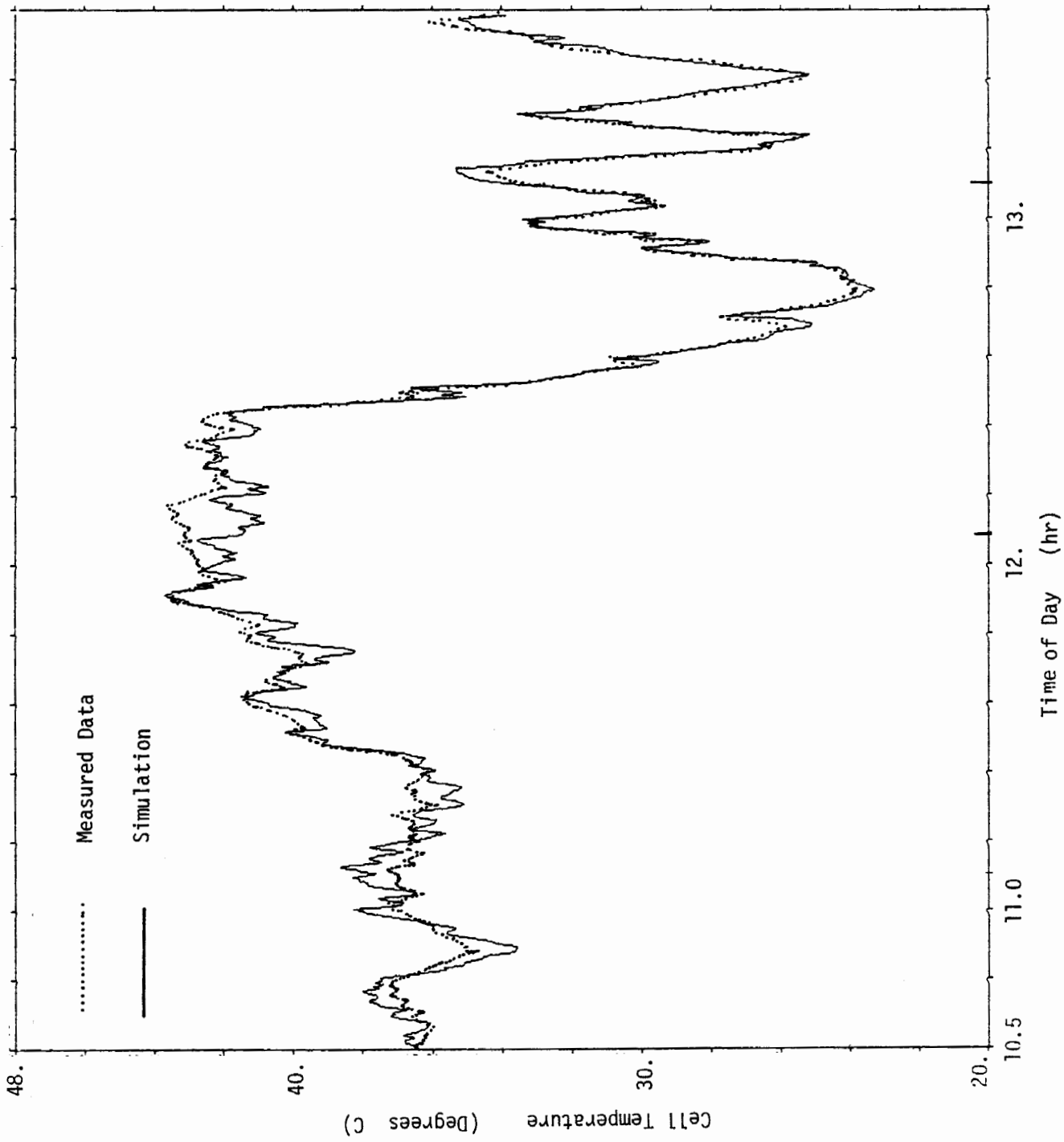


Fig. IV-1 Transient Simulation on

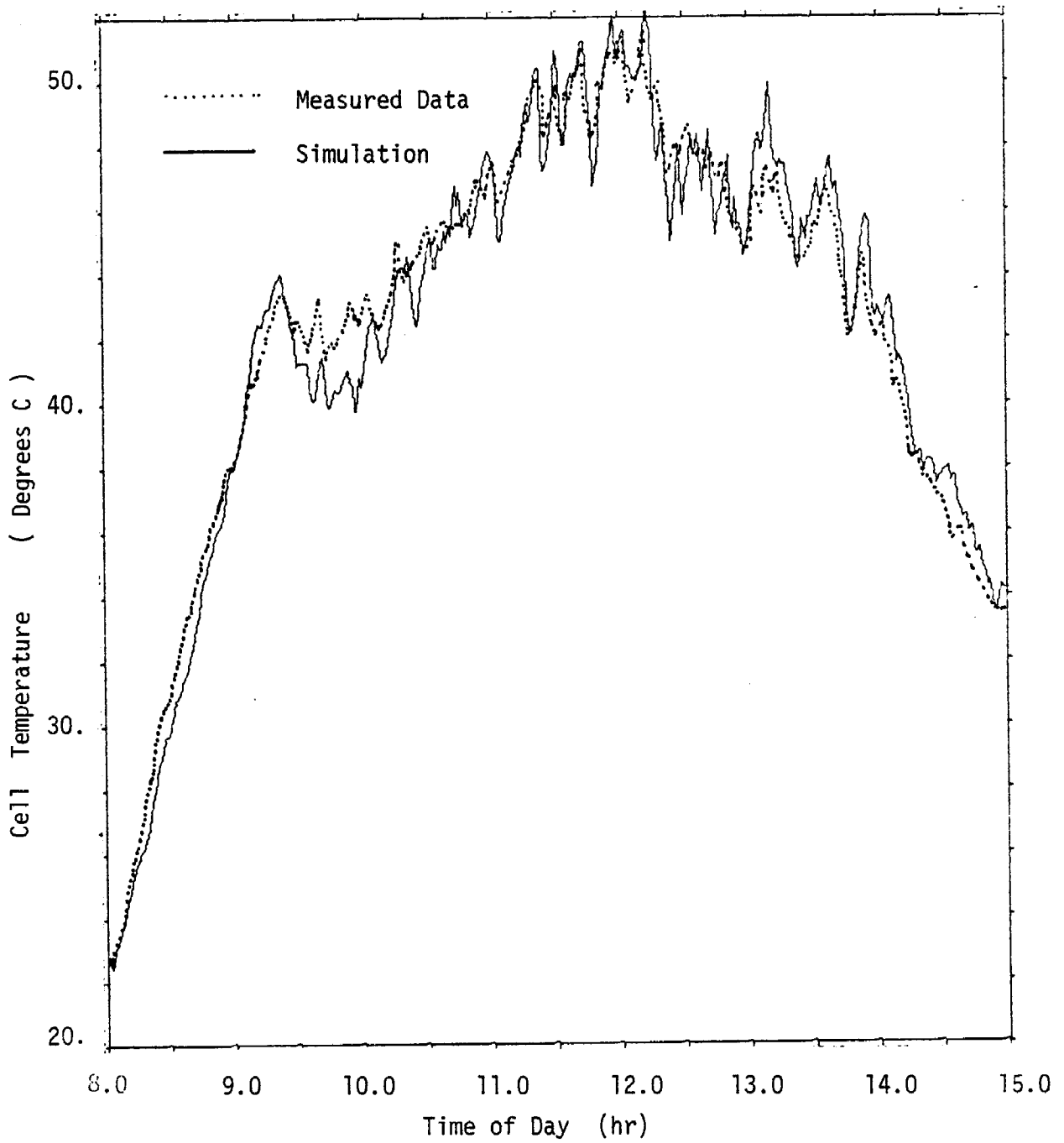


Fig. IV-2 Transient Simulation on Day

## B. ENERGY BALANCE RELATIONSHIP:

The most direct way to demonstrate the effect of an environmental factor is to assess the individual contribution to overall energy balance relationship. The absorption of incident solar energy is shown in Figure IV-3 for energy absorbed at both the front surface and that from the back surface ( with a solar absorptance of 0.39). Figure IV-4 shows the net infrared energy exchanges. It can be seen that the infrared energy absorbed from sky radiation is approximately the same order of magnitude as that absorbed from ground emission. The sum of the two is about 65% of the infrared energy emitted from the module (from both front and back surfaces). Figure IV-5 compares the net IR radiation heat loss with convective heat losses. Free convective heat loss is approximately the same magnitude as the net radiative heat loss. Forced convection loss displays a large fluctuation and its amplitude corresponds very well with the wind speed variation pattern shown in Figure II-3. The top curve in Figure IV-5 represents the total net heat loss, which is significantly different from the net energy intake from solar energy absorption shown in Fig. IV-3. The instantaneous energy balance is shown in Figure IV-6. It can be seen that the net instantaneous heat balance fluctuates drastically between the positive and negative territories. It is credited to the module thermal inertia effect that the cell temperature does not follow such rapid fluctuations.

## C. DISCUSSION:

The verification process shown here demonstrated that with carefully calibrated experimental test data, the upgraded heat transfer correlations is capable of predicting the thermal behavior very well. The uncertainty level can be reduced to around 1 degree C. However, in normal practices one would expect a larger uncertainty band in typical NOCT type test results. Data scattering for outdoor module testing can be traced to many factors, including improper treatment of the effects of local wind conditions, ground emission, ground reflection and sky radiation. The individual effects are however, having different patterns. Wind conditions fluctuates in a high frequency and is responsible for the cell temperature ripple type variations. Ground emissions and ground reflection change very gradually while sky radiation variations are determined by the cloud conditions. In terms of handling the specification and characterizations, these four parameters are also different. Sky radiations is dictated by cloud conditions. Cloudless sky radiation has been reasonably calibrated. The presence of cloud is easy to detect, but the degree of cloudiness can not be effectively described. In order words, unless the test is performed under a cloudless sky, one may expect a scatter band in the test results. In most cases the cloud effect is less than 2 degrees C. Ground reflection of solar irradiance can be directly measured at the rear surface of the module, although it has not yet been a common practice. Ground emission is more difficult to monitor. The ground temperatures can be measured but the shadow pattern varies with time and is a complex function of the day of a year, the hour of a day and the field arrangement.

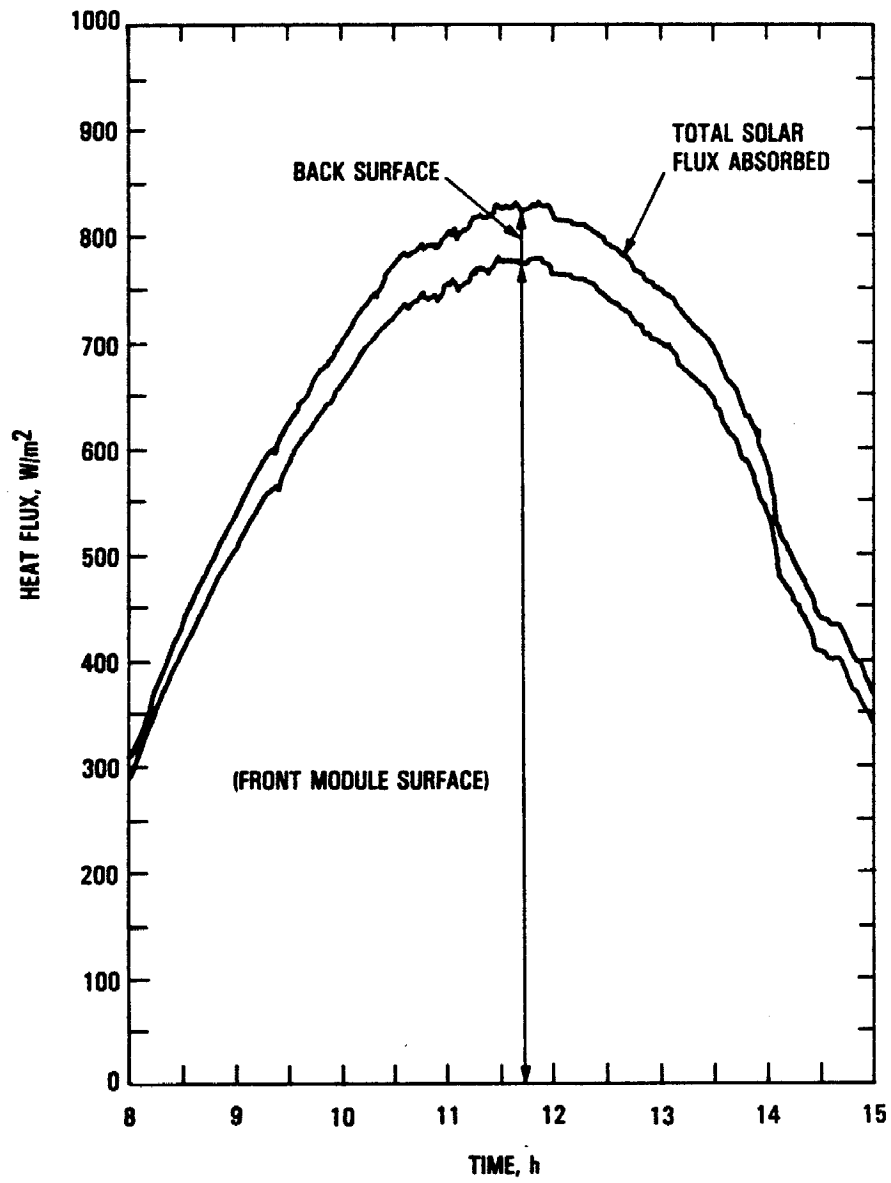


Fig. IV-3 Solar Energy Absorption by Module Surfaces

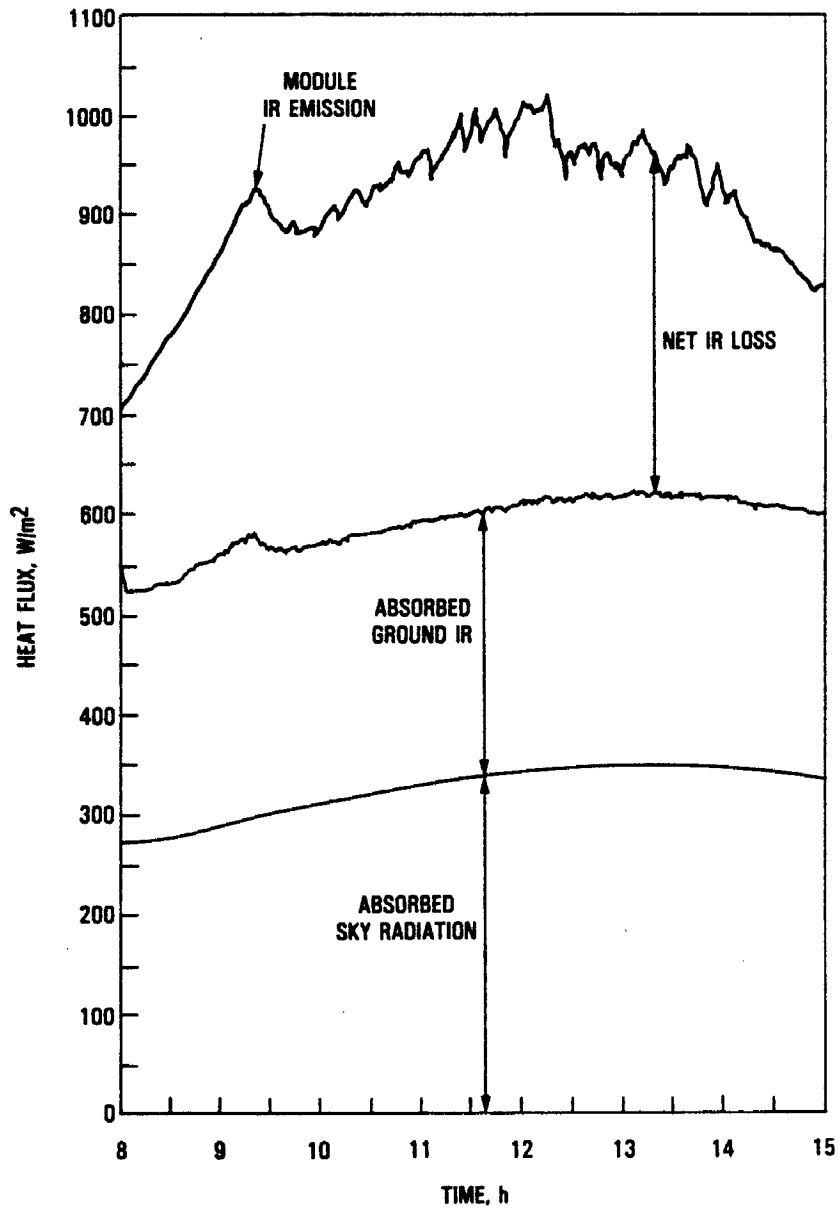


Fig. IV-4 Infrared Energy Exchanges

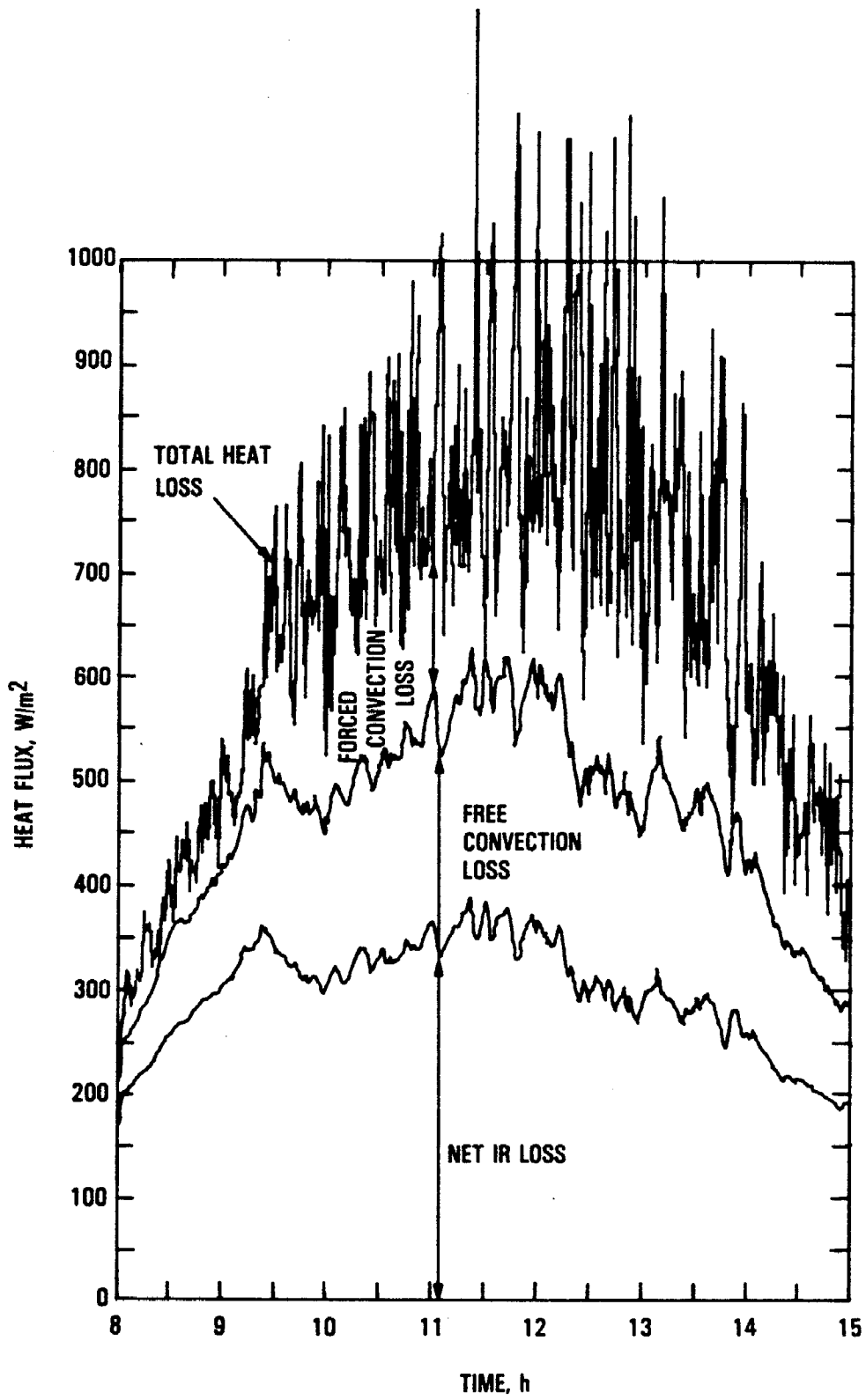


Fig. IV-5 Heat Losses from the Module Surfaces

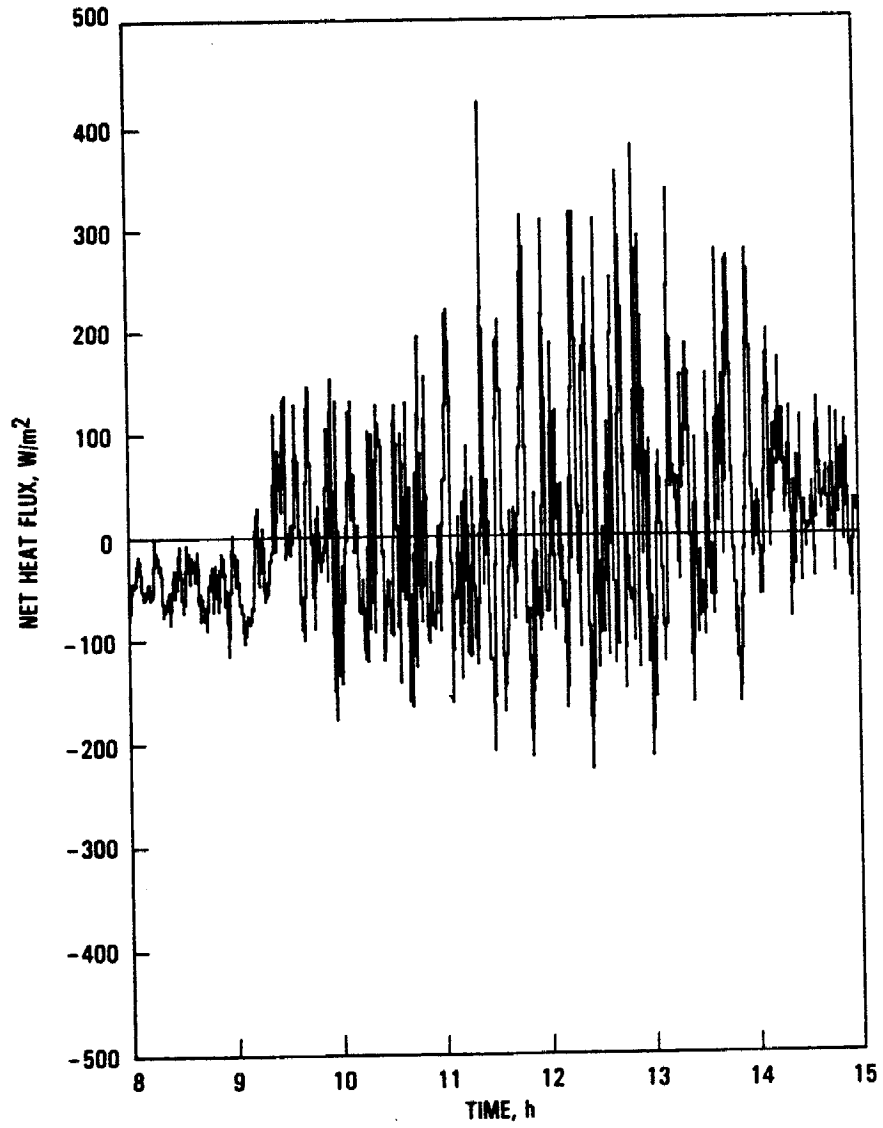


Fig. IV-6 Instantaneous Thermal Energy Balance

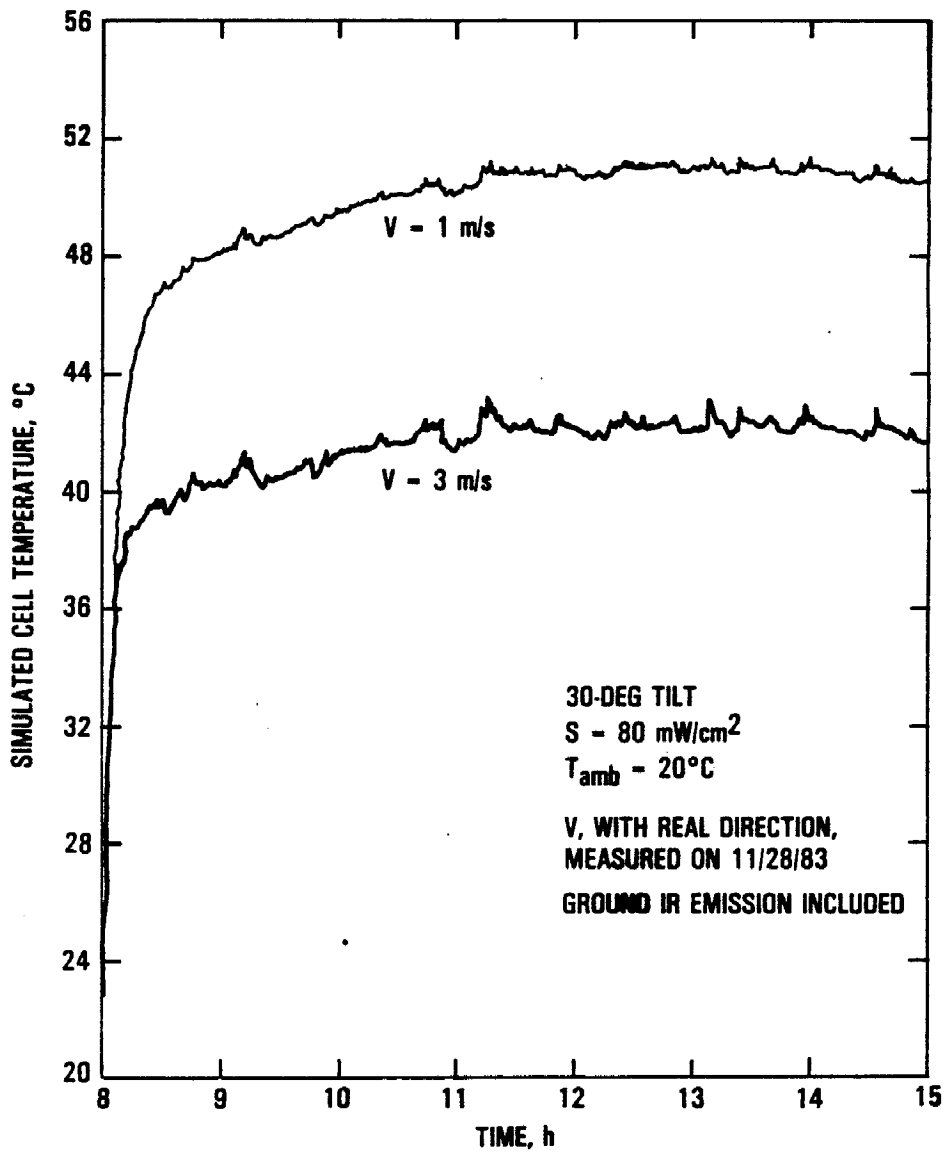


Fig. IV-7 Simulated Cell Temperature Profiles under NTE Conditions

Figure IV-7 illustrates the effects of ground emission and wind condition to simulated cell temperature profiles. It was assumed that the environmental conditions is that described by the NTE (Natural Thermal Environment) conditions of  $800 \text{ W/m}^2$  front surface insolation, 10 % ground reflection (i.e,  $80 \text{ W/m}^2$ ) to the rear surface of the module. The ambient temperature is maintained at 20 degrees C and the wind speed is kept constant at 1 m/s or 3 m/s. Actual wind directions measured on day 333,1983 was used in the simulation and is responsible of the wiggling of cell temperatures. Transient variations in ground temperature was also simulated. The predicted cell temperature can be seen to reach a plateau around 11 am. This is entirely due to the variation of ground emission which is caused by transient ground temperature variation.

Local wind condition is definitely the environmental parameter that is most difficult to handle. This is not because of its high frequency fluctuation commonly observed during tests. It was demonstrated that with properly described wind speed and directions as boundary conditions, one can accurately predict module temperature profiles. It should be pointed out that the present testing is a special case as far as wind conditions are concern. The test hardware packages were arranged very close to the anemometer and the test surfaces were left with ample air passages such that interference of wind by the structure was kept to a minimum. In many test conditions, especially with large size module or multiple module arrays the local wind conditions could be significantly different from the wind condition represented by the measurements. The result is reflected in the temperature gradient measured along the arrays. The variation of wind with altitude inside the layer near the ground has been shown to fit a power law correlations. The coefficient varies from the well known  $1/7$ th power to a higher ratio around  $1/2.5$ . The effective wind distribution around a large array is even more complicated. The center of the array could have a stagnant air layer while the local air movement near the edge could accelerate and has a higher speed than the free-stream value.

## REFERENCES

- (1) Stultz, J. W. and Wen, L., ' Thermal Performance Testing and Analysis of Photovoltaic Modules in Natural Sunlight ' JPL Internal Report No. 5101-31, Jet Propulsion Laboratory, Pasadena, CA. July 29, 1977
- (2) Wen, L., ' Thermal performance of Residential Photovoltaic Arrays ' presented at ASES meeting, Anaheim, CA., June 7, 1984
- (3) Stultz, J. W., ' Thermal and Other Tests of Photovoltaic Modules Performed in Natural Sunlight ' JPL Report 5101-76 and DOE/JPL-1012-78/9, July, 1978
- (4) Smith, J. P., ' SINDA User's Manual ' Report No.14690-H881-R0-00, Systems Group, TRW System, 1974
- (5) Gilmore, M. R., ' Thermophysical Properties of Eleven JPL Solar Panels ' - private communication, March 1983
- (6) Smokler, M. I., ' User Handbook for Block IV Silicon Solar Cell Modules ' DOE/JPL-1012-75, Sept.1 1982
- (7) Raithby, G. D. and Hollands, H. G. T., ' A General Method of Obtaining Approximate Solutions to Laminar and Turbulent Free-Convection Problems ' Advances in Heat Transfer, Vol.11, pp. 265-315, Edited by T. F. Irvine and J. P. Hartnett, Academic Press, 1975
- (8) Fussey, D. E. and Warneford, I. P., ' An Analysis of Laminar Free Convection From an Upward-facing Inclined Flat Plate ' Letter Heat and Mass Transfer', Vol. 3, pp. 443-448, 1976
- (9) McAdams, W. H., ' Heat Transmission ', 3rd Edition, McGraw-Hill Book Co. Inc., New York, 1954
- (10) Sparrow, E. W. and Tien, K. K., ' Forced Convection Heat Transfer at an Inclined and Yawed Square Plate - application to Solar Collectors ', J. of Heat Transfer, Trans. ASME, Series C, Vol.99, pp. 507-512, 1977
- (11) Parmelee, G. V. and Huebscher, R. C., ' Forced Convection Heat Transfer from Flat Surfaces ', Report No.1316, ASHVE, 1947.
- (12) Wen, L. ' An Investigation of the Effect of Wind Cooling on Photovoltaic Arrays ' DOE/JPL-1012-69, March 1982
- (13) Griffith, J. S. Rathod, M. S. and Paslaski, J., ' Some Tests of Flat Plate Photovoltaic Module Cell Temperatures in Simulated Field Conditions ', a paper presented at the 15th IEEE Photovoltaic Specialist Conference, Kissimmee, Florida, May 12-15, 1981
- (15) Unsworth, M. H., ' Long-wave Radiation at the Ground II- Geometry of Interception by Slopes, Solids and Obstructed Planes ' Quart. J. R. Met. Soc., Vol. 101, pp. 25-34, 1975

- (16) Green, A. A., ' The Influence of Environmental Parameters on Flat Plate Solar Collector Performance ', Meteorology for Solar Energy Application Conference (C18) at the Royal Institute, International Solar Energy Society, UK Section, ISSN No. 0306-7874, 1979
- (17) Angstrom, A., ' A Study of the Radiation of the Atmosphere ' Smithsonian Miscellaneous Collections, Vol.65, No.3 City of Washington, 1915
- (18) Brunt, D., ' Notes on Radiation in the Atmosphere ', Quarterly J. of Meteor. Soc., Vol.58, pp. 389-420, 1932
- (19) Staley, D. O. and Jurica, G. M., ' Effective Atmospheric Emissivity under Clear Skies ', J. of Applied Meteorology, Vol. 11, pp. 349-356, March 1956.
- (20) Berdahl, P. and Fromberg, R., ' The Thermal Radiance of Clear Sky ', J. of Solar Energy, Vol.29, No.4, pp. 299-314, 1982
- (21) Centeno, M., ' New Formulae for the Equivalent Night Sky Emissivity ', J. of Solar Energy, Vol.28, No.6, pp. 489-498, 1982
- (22) IDso, S. B. and Jackson, R. D., ' Thermal Radiation from the Atmosphere ', J. of Geophysical Research, Vol.74, No.23, Oct.20, 1969.
- (23) Unsworth, M. H., and Monteith, J. L., ' Long-wave radiation at the ground - I. Angular distribution of incoming radiation ', pp.13-24, Quart. J. Met. Soc.(1975),101.
- (24) Duffie, J. A. and Beckman, W. A., Solar Energy and Thermal Processes, pp. 76-77, Wiley, New York, 1974
- (25) Atwater, M. A. and Ball, J. T., ' Computation of IR Sky Temperature and Comparison with Surface Temperature ', J. of Solar Energy, Vol. 21, No. 3, pp. 211-216, 1978.
- (26) Ware, J. C., ' Clear Sky Temperature ', presented at ASES meeting, Fort Collins, Colorado, Aug. 1974
- (27) Swinbank, W. C., ' Long-Wave Radiation from Clear Sky ', Quart. J. Roy. Meteor. Soc., Vol.89, 1963
- (28) Kasten, F., ' Ground Radiation as Affected by Clouds ' pp.193-195, Radiation in the Atmosphere, Edited by H.J.Bolla, Science Press, 1977.
- (29) Brunt, D., ' Physical and Dynamic Meteorology ', Cambridge Press, 1941
- (30) Kondratyev, K. Ya., ' Radiation in the Atmosphere ', Academic Press, New York and London, 1969